iScience

CellPress
OPEN ACCESS

Article

Chemotherapy but Not the Tumor Draining Lymph Nodes Determine the Immunotherapy Response in Secondary Tumors

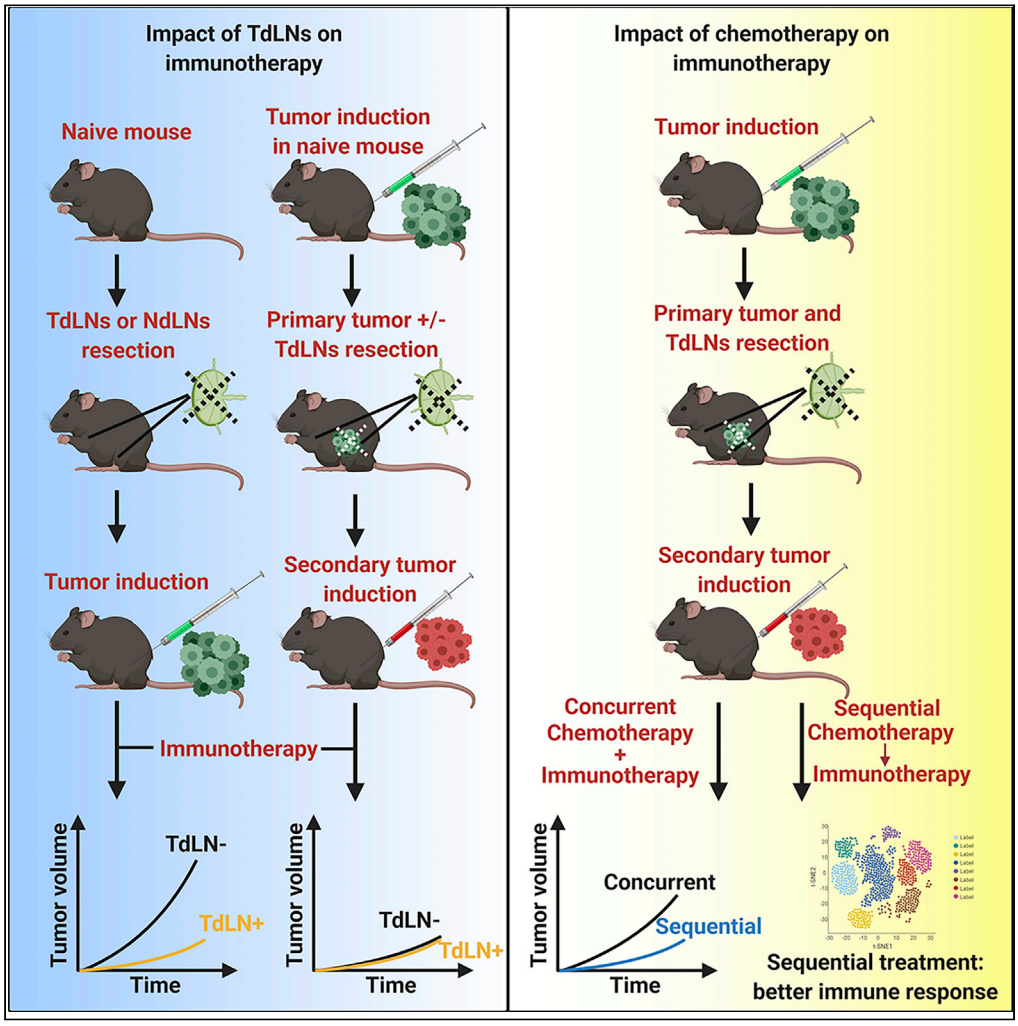

Xianda Zhao, Beminet Kassaye, Dechen Wangmo, Emil Lou, Subbaya Subramanian

subree@umn.edu

HIGHLIGHTS

During tumor progression tumor-draining lymph nodes (TdLNs) become immunotolerant

TdLNs resection with primary tumor does not affect immune response in secondary tumors

Immunoregulatory effects of chemotherapy determine immunotherapy efficacies

The sequential treatment of chemo and immunotherapies improve tumor control

Zhao et al., iScience *23*, 101056
May 22, 2020
https://doi.org/10.1016/j.isci.2020.101056

iScience

CellPress
OPEN ACCESS

Article

Chemotherapy but Not the Tumor Draining Lymph Nodes Determine the Immunotherapy Response in Secondary Tumors

Xianda Zhao,[1] Beminet Kassaye,[1] Dechen Wangmo,[1] Emil Lou,[2] and Subbaya Subramanian[1,3,4,*]

SUMMARY

Immunotherapies are used as adjuvant therapies for cancers. However, knowledge of how traditional cancer treatments affect immunotherapies is limited. Using mouse models, we demonstrate that tumor-draining lymph nodes (TdLNs) are critical for tumor antigen-specific T cell response. However, removing TdLNs concurrently with established primary tumors did not affect the immune checkpoint blockade (ICB) response on localized secondary tumor due to immunotolerance in TdLNs and distribution of antigen-specific T cells in peripheral lymphatic organs. Notably, treatment response improved with sequential administration of 5-fluorouracil (5-FU) and ICB compared with concurrent administration of ICB with 5-FU. Immune profiling revealed that using 5-FU as induction treatment increased tumor visibility to immune cells, decreased immunosuppressive cells in the tumor microenvironment, and limited chemotherapy-induced T cell depletion. We show that the effect of traditional cytotoxic treatment, not TdLNs, influences immunotherapy response in localized secondary tumors. We postulate essential considerations for successful immunotherapy strategies in clinical conditions.

INTRODUCTION

Immune checkpoint blockade (ICB) therapies (ICBTs), such as anti-CTLA-4 and anti-PD-1/PD-L1, have transformed the therapeutic landscape of cancers, including melanoma and tumors with microsatellite instability (Le et al., 2017; Robert et al., 2011; Topalian et al., 2012). Nonetheless, as with more traditional forms of systemic chemotherapy options, many patients manifest either intrinsic or acquired resistance leading to treatment failure (Gide et al., 2018; Sharma et al., 2017; Zhao and Subramanian, 2017). Multiple mechanisms that influence tumor response to ICBTs have been identified—the mutational load in tumor cells, degree of T cell exhaustion, tumor microenvironmental functions, and intestinal microbiota (Gide et al., 2018; Sharma et al., 2017; Zhao and Subramanian, 2017). In most cases, ICBT is used for treating patients with heavily pre-treated tumors. The interactions between first-line therapy may influence tumor response to subsequently administered ICBTs owing to tumor evolution and heterogeneity. In most patients with solid tumors, common interventions before ICBT include resection of primary tumors with concurrent resection of draining lymph nodes followed by administration of chemotherapies and/or targeted therapies (Le et al., 2017; Lee et al., 2017; Rizvi et al., 2015). However, minimal information is known about whether these interventions will impact tumor response to ICBT.

Tumor-draining lymph nodes (TdLNs), which are usually resected concurrently with the primary tumors, have shown dual impacts on tumor development and treatment. On the one hand, TdLNs are critical peripheral lymphatic organs where tumor antigens are presented by dendritic cells to naive T cells to elicit antitumor immunity (Fisher and Fisher, 1971; Shu et al., 2006; Toki et al., 2020). Thus, loss of TdLNs weakens immunosurveillance mechanisms and increases the likelihood of tumor initiation and progression (Fisher and Fisher, 1971; Karlsson et al., 2010; Shu et al., 2006; Toki et al., 2020). On the other hand, TdLNs are affected by immunosuppressive factors released by tumor cells during tumor progression. These immunosuppressive factors can suppress the function of TdLNs, making them immune-privileged sites (Cochran et al., 2001; Ito et al., 2006; Munn and Mellor, 2006; Murthy et al., 2019; Watanabe et al., 2008). Based on these facts, we hypothesize that TdLNs resection is an essential factor that influences long-term tumor immunity and response to ICBT. In this study, we used tumor models representing different disease stages to

[1]Department of Surgery, University of Minnesota Medical School, 11-212 Moos Tower, Mayo Mail Code 195, 420 Delaware Street SE, Minneapolis, MN 55455, USA

[2]Department of Medicine, University of Minnesota Medical School, Minneapolis, MN 55455, USA

[3]Masonic Cancer Center, University of Minnesota, Minneapolis, MN 55455, USA

[4]Lead Contact

*Correspondence: subree@umn.edu

https://doi.org/10.1016/j.isci.2020.101056

elucidate the impacts of TdLNs resection on ICBT efficacy and understand the underlying mechanisms of those effects.

The immunoregulatory effects of chemotherapies have been investigated in multiple cancer models with different chemotherapy drugs. Chemotherapy drugs such as oxaliplatin, paclitaxel, and 5-fluorouracil (5-FU) have shown positive effects in antitumor immunity either by eliciting a tumor-specific T cell response or by reducing immunosuppressive factors in the tumor microenvironment (Khosravianfar et al., 2018; Pfirschke et al., 2016; Zhang et al., 2008). Bone marrow suppression, which is a common side effect of chemotherapies, causes leukopenia that affects antitumor immunity. Because chemotherapies have dual effects on regulating antitumor immunity, we hypothesize that combining chemotherapy with ICBT has diverse effects on antitumor immune response and, consequently, an appropriate combinatory strategy will be critical in determining tumor response. In this study, we used 5-FU, which blocks DNA replication, as a representative chemotherapeutic drug to study the factors that influence the effects of chemotherapy on ICBT.

Mouse models are critical for pre-clinical cancer studies; most published studies have been performed on primary tumor models. To better represent the clinical conditions in which most immunotherapies are administered, we established a mouse tumor model that allows evaluation of the immunotherapeutic response in secondary tumors after primary tumor resection with or without concurrent TdLNs removal. We also included anti-PD-1 (antagonist to inhibitory immune checkpoints) and anti-4-1BB (agonist to stimulatory immune checkpoints) to better represent ICBT with different mechanisms (Buchan et al., 2018; Chester et al., 2016).

RESULTS

TdLNs Are Essential for Antitumor Immune Activation and Immunotherapy Response in Early-Stage Disease

We first needed to identify TdLNs in the subcutaneous tumor model. We injected Evans blue and Alexa Fluor® 488 into tumors established in the right flank of the mice to trace lymphatic drainage (Figure S1A). Evans blue staining was detected in the right inguinal and axillary lymph nodes 10 min after injection (Figure S1B). To develop a more sensitive method for detection, we used flow cytometry to trace the Alexa Fluor 488 drainage in lymphatic organs for up to 48 h. Again, the right inguinal and right axillary lymph nodes showed the highest fluorescence intensity (Figure S1C). Other lymph nodes, such as right brachial and right popliteal lymph nodes, also showed increased fluorescence signal after injection, but the signal intensity was significantly lower than in the right inguinal and right axillary lymph nodes (Figure S1C). Also, increased weight was observed in the spleen, and right inguinal and axillary lymph nodes during tumor development, suggesting an immune response occurred in these lymphatic organs (Figures S2A–S2J). Collectively, these results indicated that the right inguinal and right axillary lymph nodes are the sentinel TdLNs in our tumor model.

Next, we evaluated the impact of TdLNs on tumor initiation and antitumor immune response stimulation. Resection of TdLNs, but not non-draining lymph nodes (NdLNs), before tumor cell inoculation significantly accelerated tumor development in both CT26 and MC38 tumor models (Figure 1A). We then analyzed the stimulation of antitumor immunity with and without TdLNs. We used the frequency of tumor antigen-specific $CD8^+$ T cells (10 days after tumor cells inoculation) as an indicator of antitumor immune response stimulation (Figure S3). More tumor antigen-specific $CD8^+$ T cells were detected in the right and left brachial lymph nodes and spleen of tumor-bearing mice with intact TdLNs (Figure 1B). 4-1BB (CD137) provides important co-stimulatory signaling for T cells, and its agonist has shown tumor-eliminating effects in mice (Chester et al., 2016). To test the effects of TdLNs on the immunotherapeutic response, we administered two injections of anti-4-1BB shortly after tumor cell inoculation to simulate patients with minimal disease burden. The prophylactic anti-4-1BB treatments successfully prevented tumor development in mice with intact TdLNs, and anti-tumor immunity memory was established as evidenced by their rejection of secondary tumors. These effects were not seen in mice with resected TdLNs (Figure 1C). These data demonstrated that TdLNs are critical for anti-tumor immunity activation and loss of TdLNs leads to rapid early-stage tumor growth even with the potent T cell co-stimulatory agonist.

TdLNs Are Not Necessary for Immunotherapy Response in Advanced Disease Tumor Models

Since recurrence after primary tumor resection is one of the major causes for treatment failure, we evaluated the impact of TdLNs on tumor recurrence and the response to immunotherapy in mouse models after

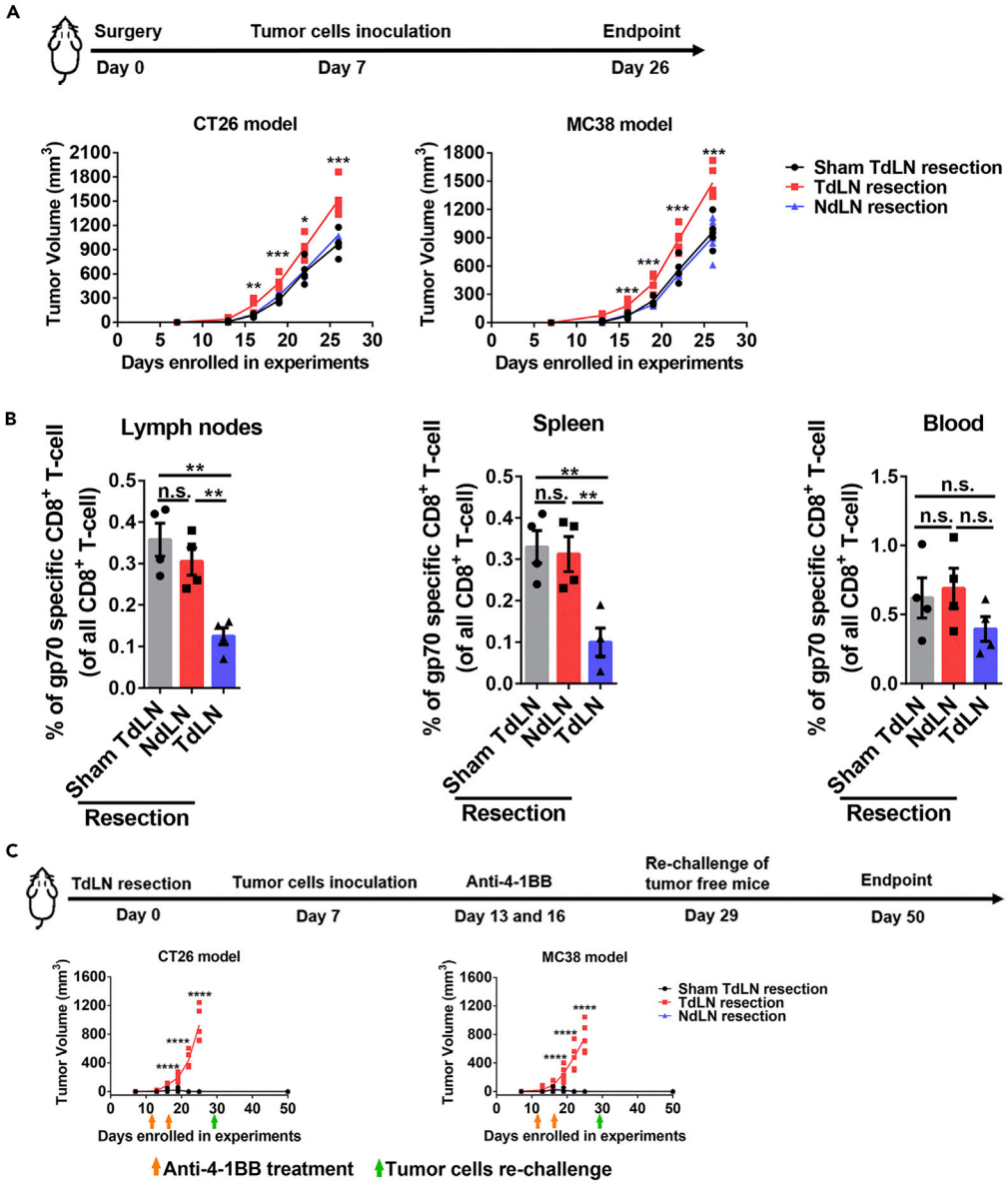

Figure 1. Impact of TdLNs on Tumor Initiation and Immunotherapy Response in Early-Stage Tumor Models

(A) Experimental schedule and tumor growth curves in mice with or without TdLNs. Both CT26 (BALB/c mouse as the host) and MC38 (C57BL/6 mouse as the host) subcutaneous models were enrolled in the experiment. Mice were pre-conditioned by TdLNs resection (right inguinal and axillary LNs), NdLNs resection (left inguinal and axillary LNs), or sham surgery prior to tumor inoculation. Accelerated tumor growth was observed in mice without TdLNs (n = 5 in each group, one-way ANOVA test between all groups, data represent each individual mouse, *$p < 0.05$, **$p < 0.01$, ***$p < 0.001$).

(B) Distribution of tumor antigen (gp70)-specific $CD8^+$ T cells in tumor-bearing mice with or without TdLNs. Fewer tumor antigen-specific $CD8^+$ T cells were detected in right and left brachial lymph nodes and spleen of TdLNs resected tumor-bearing mice (n = 4 in each group, Tukey's multiple comparisons test between two groups, data were displayed as means ± SEMs, n.s.: no significance, **$p < 0.01$).

(C) Experimental schedule and early-stage tumor response to anti-4-1BB treatment. Two injections of anti-4-1BB were given shortly after tumor inoculation. The treatment prevented tumor development in tumor-bearing mice with intact TdLNs. Rechallenge of the tumor cells did not form tumors in all anti-4-1BB cured mice (n = 4 in each group, one-way ANOVA test between all groups, data represent each individual mouse, ****$p < 0.0001$).

See also Figures S1–S3 and Table S1.

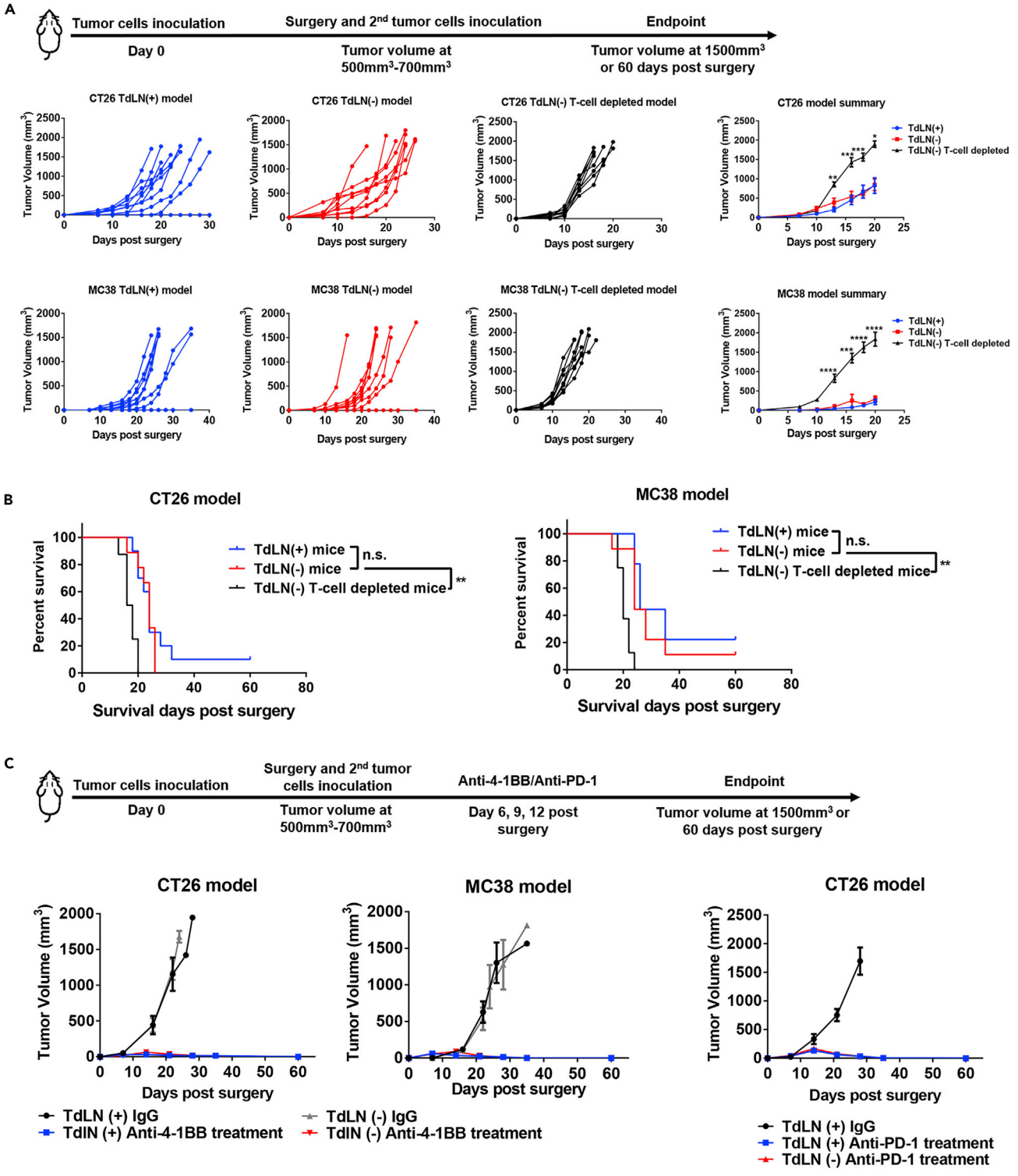

Figure 2. Impact of TdLNs on Tumor Recurrence and Immunotherapy Response in Advanced Stage Tumor Models

(A) The experimental schedule. Resection of TdLNs did not accelerate localized secondary tumor (mimicking recurrent tumor) development in both CT26 and MC38 subcutaneous tumor models. However, systemic deletion of T cells significantly accelerated secondary tumor development in both tumor models (n = 8–10 in each group, both individual and summarized curves were shown, t tests were performed between the TdLN resected and T cell-depleted groups,

Figure 2. *Continued*

data were displayed as means ± SEMs, t test was performed between the TdLN(−) and TdLN(−) T cell-depleted groups, *p < 0.05, **p < 0.01, ***p < 0.001, ****p < 0.0001).

(B) Systemic depletion of T cells, but not TdLN resection, led to a shorter survival time of mice owing to secondary tumor development (n = 8–10 in each group, log rank test between indicated groups, **p < 0.01).

(C) Response to anti-4-1BB and anti-PD-1 treatment was tested in localized secondary tumors with or without TdLNs. Anti-4-1BB and anti-PD-1 treatments suppressed secondary tumor growth in both TdLN intact and resected mice (n = 5 in each group, data were displayed as means ± SEMs).

See also Figures S1, S2, and S4, and Table S1.

advanced primary tumor resection. We allowed the primary tumor to grow to a relatively large volume and then resected the primary tumor with and without concurrent TdLNs resection. Secondary tumors were then inoculated to mimic localized tumor recurrence (Figure 2A). We confirmed a clean primary tumor resection margin in our models (Table S1), allowing all secondary tumors to start with a comparable baseline. TdLNs were also subjected to histological analysis to confirm that no metastasis developed in TdLNs (Figure S2K). Notably, in our well-controlled model, the secondary tumor growth rate was similar in mice with and without TdLNs (Figures 2A and 2B). In another group of TdLNs resected mice, we depleted T cells to study the impact of systemic immunity on subsequent tumor development. As predicted, the secondary tumor developed rapidly in mice with impaired systemic immunity (Figures 2A and 2B). Together, these results indicate that tumor recurrence is accelerated by impaired systemic immunity but not by impaired regional immunity (TdLNs resection).

Next, we asked whether TdLNs resection altered immune infiltration in secondary tumors. The major immune cell types were evaluated in secondary tumors (Figure S4). Total tumor-infiltrating T cells, PD-1 high expression T cells, and MDSCs were not altered in secondary tumors either with or without TdLNs. PD-L1 expression was similar. The frequency of $CD103^+$ DCs and lymphatic endothelial cells was significantly higher in the secondary MC38 tumors with TdLNs (Figure S4). However, in the CT26 model, only the lymphatic endothelial cell frequency was statistically higher in secondary tumors with TdLNs than in those without TdLNs. The frequency of $CD103^+$ DCs showed a similar trend but did not reach statistical significance (Figure S4).

Immunotherapies are typically prescribed to patients who have undergone advanced primary tumor resection. In another pre-clinical model, we administrated anti-4-1BB and anti-PD-1 to study whether TdLN resection will lead to immunotherapy resistance. To mimic clinical conditions, we resected the established primary tumor both with and without concurrent TdLN resection. We then inoculated the secondary tumor to mimic localized tumor recurrence. A 6-day gap was allowed between the secondary tumor inoculation and any treatment (Figure 2C). This allows the tumor to connect with systemic circulation and to establish the tumor microenvironment. Then, the mice were treated with anti-4-1BB or anti-PD-1 (Figure 2C). Notably, both anti-4-1BB and anti-PD-1 treatments were efficient in controlling secondary tumor initiation. Secondary tumor control was maintained after TdLNs resection (Figure 2C), suggesting that TdLN resection may not be a major influencing factor on the efficacy of ICBT when used as adjuvant therapy in late-stage disease.

TdLNs Shift from an Immunoactive to an Immunotolerant Environment and Tumor-Antigen Specific T Cells Disseminate during Tumor Development

Based on the above results, we then hypothesized that immunosuppression in TdLNs and systemic spreading of tumor antigen-specific T cells during tumor development make the TdLNs less important for late-stage tumors compared with early-stage tumors. We collected the TdLNs and NdLNs at different stages of tumor development for analysis and compared them with the naive lymph nodes (LNs). The frequency of $CD62L^-$ $CD4^+$ T cells was significantly higher in TdLNs than in NdLNs when tumors were small. However, the differences disappeared once the tumors became large (Figure 3A). CD80, a crucial co-stimulatory molecule was higher on APCs in TdLNs than in NdLNs and naive LNs at early-stage disease (Figure 3B). However, with tumor development, the CD80 level on APCs in TdLNs dropped (Figure 3B). As the receptor of CD80, CD28 is highly expressed on $CD4^+$ and $CD8^+$ T cells in TdLNs of early-stage tumors but decreased dramatically during tumor development (Figure 3C). Previous studies showed that CD28 is downregulated in T cells that are repetitively exposed to antigens (Lake et al., 1993; Vallejo et al., 1999). Therefore, high numbers of T cells with lower CD28 levels may be the product of repeated activation in the TdLNs of late-stage tumors. However, recent studies indicated that sustained CD28 expression after T cell priming is required for T cell function and response to further stimulations, including immune

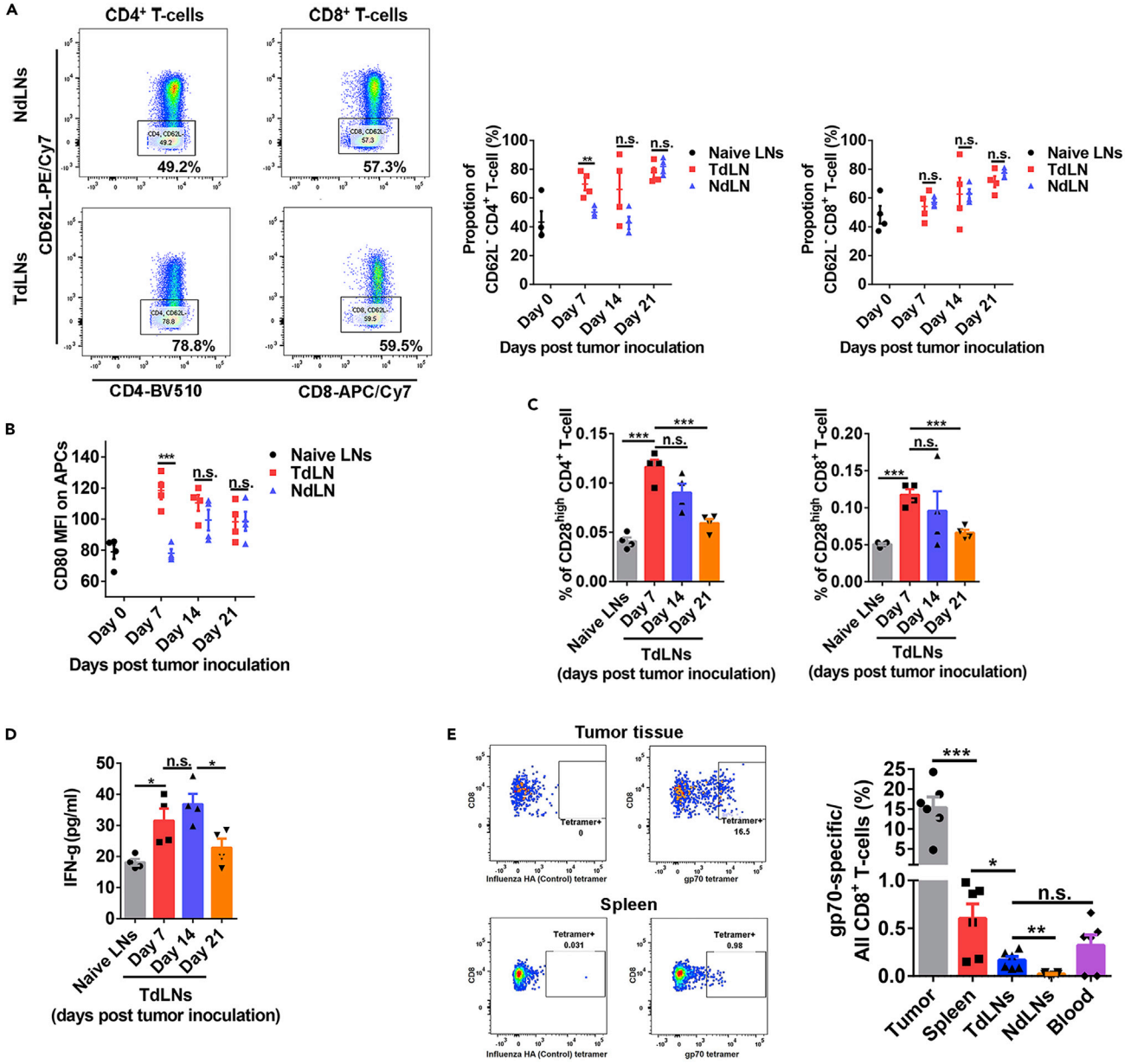

Figure 3. Functional Status of TdLNs and Tumor Antigen-Specific T cell Distribution in Tumor-Bearing Mice with Advanced Disease

(A) More activated ($CD62L^-$) $CD4^+$ T cells were observed in TdLNs than NdLNs on 7 days post tumor cells inoculation. However, at the late stage of tumor development, the proportion of activated $CD4^+$ T cells was similar in TdLNs and NdLNs. The proportion of activated $CD8^+$ T cells was close in TdLNs and NdLNs during tumor development (n = 4 in each group, t tests were performed, data were displayed as means ± SEMs, n.s.: no significance, **p < 0.01).

(B) CD80 expression level on antigen presentation cells (APCs) was higher in TdLNs than in NdLNs on 7 days post tumor cells inoculation (n = 4 in each group, t tests were performed, data were displayed as means ± SEMs, n.s.: no significance, ***p < 0.001; MFI, mean fluorescent intensity).

(C) The proportion of $CD28^{high}$ T cells (both $CD4^+$ and $CD8^+$) in TdLNs was decreased during tumor development (n = 4 in each group, t tests were performed, data were displayed as means ± SEMs, n.s.: no significance, ***p < 0.001).

(D) The concentration of IFN-γ in TdLNs was higher at the early stage of tumor development than at the late stage (n = 4 in each group, t tests were performed, data were displayed as means ± SEMs, n.s.: no significance, *p < 0.05).

(E) At the established tumor model (volume 500–700 mm^3), systemic distribution of tumor antigen (gp70)-specific $CD8^+$ T cells were detected in multiple lymphatic organs and the tumor microenvironment. The tumor microenvironment has the highest frequency of gp70-specific $CD8^+$ T cells than lymphatic organs (n = 6 in each group, t tests were performed between indicated groups, data were displayed as means ± SEMs, n.s.: no significance, *p < 0.05, **p < 0.01, ***p < 0.001).

See also Figures S1–S3 and Table S1.

checkpoint inhibitors (Kamphorst et al., 2017; Linterman et al., 2014). IFN-γ is highly produced by functional T cells. However, decreased IFN-γ concentration was observed in TdLNs during tumor development (Figure 3D). These data suggested that immune cells in TdLNs of late-stage tumors may not function as properly as in the TdLNs of early-stage tumors, shifting the TdLNs from an immunoactive to the immunotolerant environment during tumor development.

The amount and distribution of tumor antigen-specific T cells also influence antitumor immunity and immunotherapy response (Liu et al., 2016). We measured the distribution of tumor antigen-specific T cells in mice with established tumors (volume 500–700 mm^3) (Figure S3). As expected, the frequency of gp70-specific $CD8^+$ T cells was highest in the tumor-infiltrating $CD8^+$ T cells population. The gp70-specific $CD8^+$ T cells were detected in all major peripheral lymphatic organs, including spleen, TdLNs, NdLNs, and blood (Figure 3E). The proportion of $CD4^+$ (around 55%–65% of all T cells) and $CD8^+$ (around 25%–35% of all T cells) T cells in TdLNs was comparable with that in the naive mice LNs (data not shown). Considering that TdLNs are only a very small proportion of the lymphatic system, our data suggested that in advanced tumor conditions, TdLNs are not the primary reservoir of tumor antigen-specific T cells. The widely distributed tumor antigen-specific T cells in peripheral lymphatic organs could be the responders of immunotherapies for controlling localized residual tumor (minimal secondary tumors in our model) recurrence.

Sequential Treatment of 5-FU and Anti-4-1BB or Anti-PD-1 Leads to Better Responses Than Concurrent Treatment

In addition to the primary tumor and TdLNs resection, chemotherapy is a critical factor potentially affecting the efficacy of immunotherapies. Since our preceding data showed that TdLN resection may not affect the immunotherapeutic response, we then focused on the impacts of chemotherapy on immunotherapies. Several mechanisms by which chemotherapies regulate anti-tumor immunity have been identified (Emens and Middleton, 2015; Fend et al., 2017; Galluzzi et al., 2017; Pfirschke et al., 2016). However, no study has analyzed whether the schedule of combining chemotherapies with immunotherapies influences their synergetic effects. To investigate the impact of different combination therapy schedules on tumor response, we compared sequential versus concurrent 5-FU and anti-4-1BB or anti-PD-1 therapy in mouse models. The IgG and anti-4-1BB monotherapy in immunocompetent and T cell-depleted mice served as control groups (Figure 4A). In mice with established tumors, anti-4-1BB monotherapy delayed tumor growth and prolonged mice survival time (Figures 4B and 4C). Anti-CD3 impaired systemic immunity by suppressing T cell populations (Figure S5). In an established tumor model, anti-CD3 preconditioning nullified the anti-tumor effects of anti-4-1BB (Figures 4B and 4C), indicating that intact systemic immunity was required for anti-4-1BB response. 5-FU also delayed tumor development in established tumor models (Figures 4B and 4C). We then combined anti-4-1BB with the 5-FU treatment and found no noticeable improvement in mice survival time (Figures 4B and 4C). In another cohort of mice, the 5-FU treatment was used as induction, and then later, anti-4-1BB was added as the maintenance treatment (Figures 4B and 4C). To determine an appropriate sequential treatment strategy, we tested the dynamics of 5-FU-induced T cell depletion (Figure S5). In the sequential treatment, anti-4-1BB was given when the T cell population had almost recovered from the 5-FU treatment. Mice treated with sequential combination therapy had the longest survival time and the most effective tumor control of all cohorts (Figures 4B and 4C).

Next, we compared the 5-FU and anti-4-1BB sequential and concurrent treatments in a more clinically relevant model. In this model, we performed resection of the established primary tumor together with its TdLNs and induced localized secondary tumors for treatment (Figure 5A). Over 60 days of the experiment, the sequential treatment showed better tumor suppression than concurrent treatment (Figure 5B). Anti-PD-1 is an FDA-approved class of cancer-directed immunotherapy with different mechanisms than anti-4-1BB. To test whether the conclusion from the anti-4-1BB treatment was generalizable to the anti-PD-1 treatment, we combined 5-FU and anti-PD-1 in concurrent and sequential schedules. Again, the 5-FU and anti-PD-1 given in sequence showed better tumor control than when administered concurrently (Figure 5C).

Toxicity is a primary concern for cancer treatments, especially in combination therapy. We took this into account by evaluating the side effects of each treatment. 5-FU monotherapy and 5-FU and anti-4-1BB concurrent combination therapy caused severe body weight loss and diarrhea during the treatment (Figure S6). In contrast, the 5-FU and anti-4-1BB sequential combination therapy showed slight or no side effects for the duration of the experiment (Figure S6).

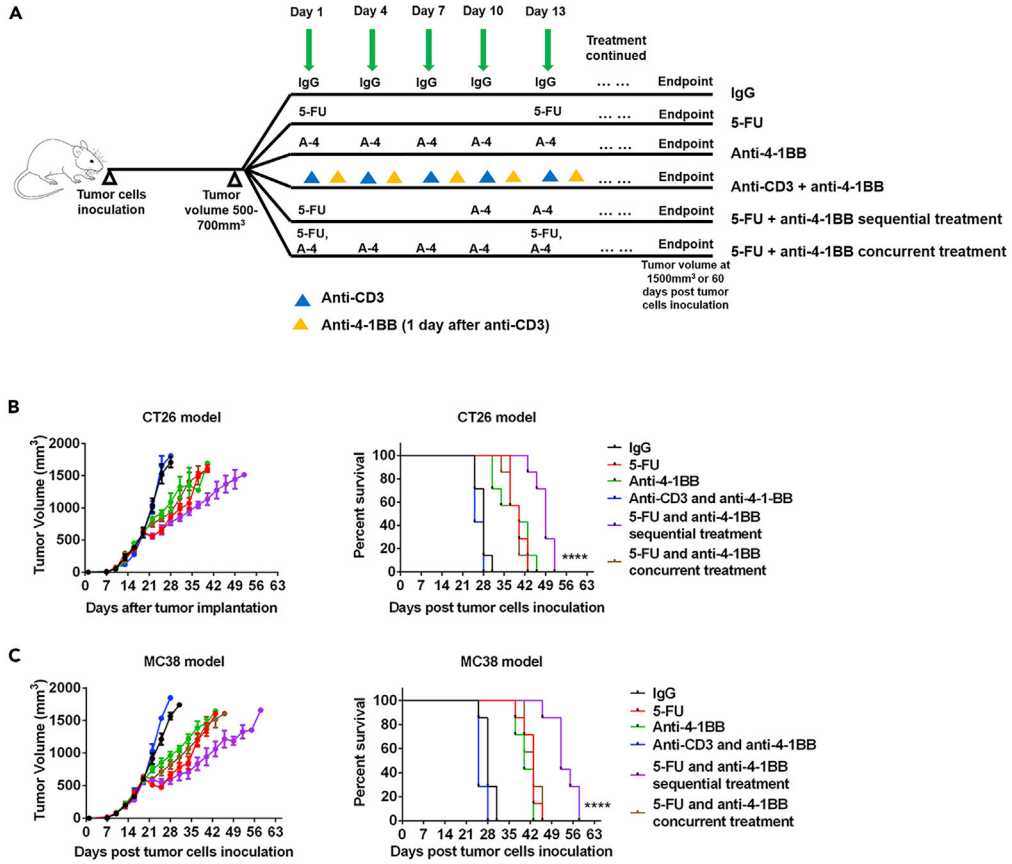

Figure 4. 5-FU and Anti-4-1BB Sequential Treatment Elicits Strong Antitumor Activity

(A) Tumor (500–700 mm^3 in volume) bearing mice were randomly assigned to six treatment groups: IgG (one dose/3 days), 5-FU monotherapy (one dose/12 days), anti-4-1BB monotherapy (one dose/3 days), anti-CD3 therapy (one dose/3 days) and anti-4-1BB therapy (one dose/3 days, two days after anti-CD3), 5-FU (one dose) and anti-4-1BB (1 dose/3 day, starting at 9 days post 5-FU) sequential therapy, and 5-FU (one dose/12 days) and anti-4-1BB (1 dose/3 day, started at the same day of 5-FU) concurrent therapy. The treatment was continued until the endpoint of follow-up.

(B) CT26 tumor response to different treatments. The 5-FU and anti-4-1BB sequential treatment significantly prolonged survival time of the tumor-bearing mice (n = 4 in each group for the tumor growth curve, data were displayed as means ± SEMs, n = 7 in each group for the mouse survival curve, log rank test between all survival curves, ****$p < 0.0001$).

(C) The same experiments of (B) were repeated in the MC38 tumor model (n = 4 in each group for the tumor growth curve, data were displayed as means ± SEMs, n = 7 in each group for the mouse survival curve, log rank test between all survival curves, ****$p < 0.0001$).

See also Figures S5 and S6.

Sequential Treatment of 5-FU and Anti-4-1BB or Anti-PD-1 Stimulates a Strong Antitumor Immune Response

Our pre-clinical models suggested that 5-FU and anti-4-1BB or anti-PD-1 sequential treatment has superior tumor controlling effects than the concurrent treatment schedule. We investigated the potential mechanisms of this result by performing mass cytometry to generate a comprehensive immune landscape characterization in tumor tissues (Figure S7). Notably, CD80 and CD86 expression were upregulated after 5-FU and anti-4-1BB sequential treatment in CT26 tumors (Figure 6A). High expression of these two critical co-stimulatory factors suggests enhanced tumor visibility by T cells. The expression of PD-L1 on tumor tissue was not significantly changed among different groups (Figure 6A). Furthermore, tumor immune infiltration studies showed that anti-4-1BB monotherapy stimulated tumor-infiltrating T cell proliferation and increased the $CD8^+$ T cell versus regulatory T cell ratio (Figures 6B–6D). In sum, these experiments showed that 5-FU and anti-4-1BB sequential treatment alone maintained the positive effects of anti-4-1BB on the T cell population (Figures 6B–6D).

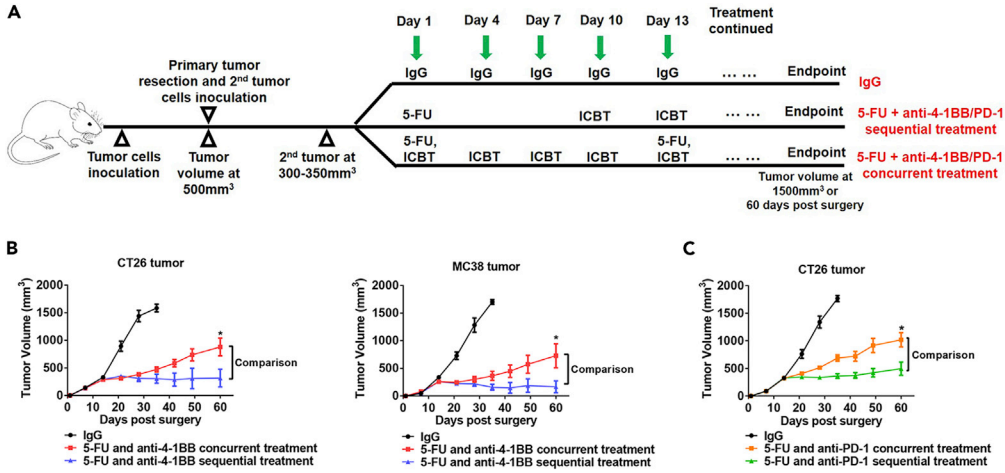

Figure 5. 5-FU and Anti-4-1BB Sequential Treatment on Secondary Tumors that Mimic Tumor Recurrence

(A) The primary tumor and TdLNs were resected when tumors are at around 500 mm^3 in volume. Secondary tumors were induced and treated by different strategies at 300–350 mm^3 in volume. Some mice rejected the secondary tumors and were not included in the therapeutic study (anti-4-1BB or anti-PD-1).

(B) The 5-FU and anti-4-1BB sequential treatment was more efficient than the 5-FU and anti-4-1BB concurrent treatment in controlling secondary tumors in CT26 and MC38 models (n = 7 in each group, data were displayed as means ± SEMs, t test was performed between the sequential and concurrent treatment groups, *$p < 0.05$).

(C) The 5-FU and anti-PD-1 sequential treatment was more efficient in controlling secondary tumors than the 5-FU and anti-PD-1 concurrent treatment in the CT26 model (n = 7 in each group, data were displayed as means ± SEMs, t test was performed between the sequential and concurrent treatment groups, *$p < 0.05$).

See also Figure S5.

Meanwhile, the tumors treated by the sequential therapy had the lowest MDSC frequency and highest NK cell frequency (Figures 6F and 6H). PD-1 expression on $CD8^+$ T cells and macrophages frequency was similar among all groups (Figures 6E and 6G). $CD103^+$ DC frequency trended higher in the anti-4-1BB monotherapy group but was not statistically significant (Figure 6I). We repeated the same experiment in MC38 tumors (Figure S8) and obtained similar results as in CT26 tumors with most parameters tested. However, CD80 and CD86 expression levels in MC38 tumors were not increased significantly by 5-FU and anti-4-1BB sequential treatments. This difference between MC38 and CT26 tumors indicates the tumor-dependent effects of the treatment. In CT26 tumors, we also evaluated the immunoregulatory effects of 5-FU and anti-PD-1 combination (Figure S9). Tumor-wide expression of PD-L1, CD86, and CD80 was increased in 5-FU and anti-PD-1 sequential treatment group. In addition, the frequencies of total T cells, proliferating $CD8^+$ T cells, and NK cell was highest in tumors treated by 5-FU and anti-PD-1 sequential therapy (Figure S9). Notably, the frequency of MDSCs was decreased by 5-FU monotherapy and combination treatment (Figure S9). These findings showed the immunological impacts of different treatment strategies and reinforced that using 5-FU as an induction treatment and then anti-4-1BB or anti-PD-1 as maintenance treatments produces the most prominent and synergic effect in reversing the immunosuppressive tumor microenvironment.

DISCUSSION

Immunotherapies are mostly used as second- or third-line treatments for treatment-refractory tumors. However, studies that investigate the impact of different clinical conditions and combination strategies on tumor immunotherapy are limited. Here, we comprehensively profiled the impacts of TdLNs resection and different chemotherapy combination schedules on ICBT responses.

Surgery has been a dominant strategy for several decades to prevent, diagnose, stage, and treat cancers. Radical surgery—a procedure that removes blood supply to the tumor, lymph nodes, and sometimes adjacent structures—is routinely performed in many cancers such as colorectal cancer, breast cancer, and lung cancer. Patients with early-stage cancer have excellent disease control with surgery alone, yet advanced diseases require more comprehensive treatments, including chemotherapies, oncogenic pathway targeted therapies, and immunotherapies. Currently, most immunotherapies are used as adjuvant treatments

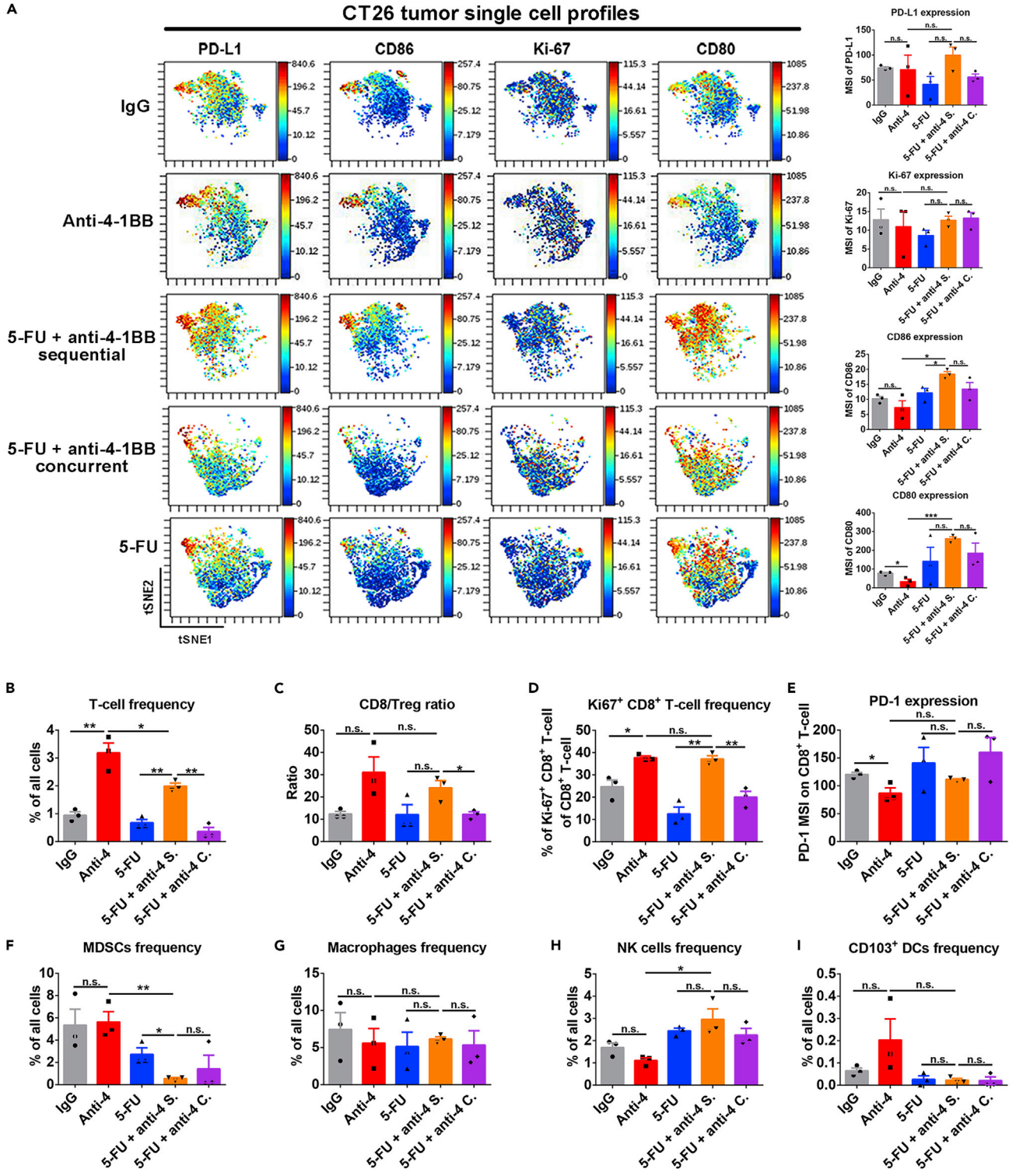

Figure 6. Tumor Immunological Response to 5-FU and Anti-4-1BB Treatments in CT26 Tumors

(A) ViSNE plot showed single cell level expression of PD-L1, Ki-67, CD80, and CD86 in the tumor tissue. PD-L1, Ki-67, CD80, and CD86 expressions were quantified in whole tumor tissue. The 5-FU and anti-4-1BB sequential treatment significantly upregulated CD86 and CD80 expression in tumor tissues (n = 3 in each group, data were displayed as means ± SEMs, t test was performed between the indicated groups, n.s.: no significance, *p < 0.05, ***p < 0.001; MSI, mean signal intensity).

Figure 6. *Continued*

(B–I) The frequencies of major tumor-infiltrating immune cell populations were measured in tumors treated by different strategies. Compared to the 5-FU and anti-4-1BB concurrent treatment, the 5-FU and anti-4-1BB sequential treatment increased T cell frequency (B), CD8/Treg ratio (C), and $Ki67^{+}CD8^{+}$ T cell frequency (D) in tumor tissues. The expression of PD-1 on $CD8^{+}$ T cells (E), myeloid-derived suppressive cells (MDSCs) frequency (F), macrophages frequency (G), NK cells frequency (H), and $CD103^{+}$ dendritic cells (DCs) frequency (I) in tumors were similar between the 5-FU and anti-4-1BB concurrent and sequential therapies (n = 3 in each group, data were displayed as means ± SEMs, t test was performed between the indicated groups, n.s.: no significance, *$p < 0.05$, **$p < 0.01$; MSI, mean signal intensity).

See also Figures S7–S9.

(given after surgeries). TdLNs are the primary lymphatic organs where antitumor immune responses are initiated (Fisher and Fisher, 1971; Jeanbart et al., 2014; Marzo et al., 1999; Munn and Mellor, 2006; Shu et al., 2006). In mouse models with resected TdLNs before tumor cell inoculation, we observed that removal of TdLNs significantly accelerated tumor growth and compromised response to immunotherapy. These data uncovered a key role for TdLNs in preventing cancer cells from evading antitumor immunity at early stages. Mechanistically, TdLNs resection in early-stage disease led to inadequate antitumor immune simulation, featured by a low frequency of tumor antigen-specific T cells in lymphatic organs. Our observations were in line with previous studies, highlighting the significance of TdLNs in initiating antitumor immunity and regulating immunotherapy response in early-stage disease (Fransen et al., 2018).

Recently, Fransen et al. reported that TdLNs are determining factors of PD-1/PD-L1 immune checkpoint therapies in early-stage tumor models (Fransen et al., 2018). However, whether the TdLNs are critical for immunotherapy response in recurrent tumor models, which represent a major clinical issue, had not been addressed. In our study, we established a model to mimic tumor recurrence from residual tumor lesions after primary tumor and TdLNs resection. We first thoroughly resected the primary tumors either with or without TdLNs resection and confirmed a clean surgical margin. We then inoculated tumor cells *in situ* to induce a secondary tumor. This method allows all secondary tumors to have a relatively similar baseline volume and growth dynamic before any treatment. We also allow the localized secondary tumors to connect with systemic circulation and establish a tumor microenvironment before treatment was initiated. Our well-designed model provided a platform for an unbiased evaluation of treatment efficacy in residual disease after primary tumor resection.

With our model, we found that resection of TdLNs in advanced tumors did not influence localized secondary tumor immunity and response to immunotherapies (anti-PD-1 and anti-4-1BB). Furthermore, we investigated the factors that determine the significance of TdLNs in antitumor immunity and immunotherapeutic response. Previous findings indicated that the bidirectional cross talk between tumor cells and TdLNs allowed remodeling of each other during tumor progression (Fisher and Fisher, 1971; Ito et al., 2006; Munn and Mellor, 2006; Shu et al., 2006; Watanabe et al., 2008). Immunosuppressive factors derived from tumors, such as TGF-β, can drain to TdLNs and induce an immunosuppressive microenvironment (Cochran et al., 2006; Ito et al., 2006). We tested the hypothesis that antitumor function of TdLNs is impaired in advanced tumor models. We compared the immune responses in naive LNs and TdLNs of early-stage and advanced tumors and demonstrated a trend between potent immunosuppression in TdLNs and tumor progression. Although the TdLNs eventually became immunotolerant, the distribution of tumor antigen-specific T cells are extensive in lymphatic tissues in advanced tumors. Resection of TdLNs did not significantly reduce the population of tumor-antigen-specific T cells that respond to immunotherapies. Our data corroborate with previous reports showing strong immunosuppression development in TdLNs of human cancers (Murthy et al., 2019; Shuang et al., 2017). This explains why resection of TdLNs may not influence the antitumor immunity in late-stage tumor models. Finally, it is also important to understand that the resected TdLNs in our experimental models might have developed immunotolerance. However, since humans have more TdLNs than the mouse model, immunoactive TdLNs do exist in certain circumstances and might influence immunotherapy response (Toki et al., 2020; Wu et al., 2014). Therefore, it will be critical to evaluate the functional status of TdLNs in humans before extending our conclusions to human cancers.

Systemic therapies, such as chemotherapies are used to treat primary tumors, eradicate micrometastatic disease, or stabilize the disease in widespread incurable conditions (DeVita and Chu, 2008). Chemotherapies have the advantages of being fast acting and effective; thus, they are widely administered as the primary treatment for combinational strategies (DeVita and Chu, 2008). Combinations of chemotherapies with immunotherapies are extensively discussed and currently tested in pre-clinical models and clinical trials (Emens and Middleton, 2015; Kareva, 2017; Pfirschke et al., 2016; Wang et al., 2018). Comprehensive

studies have revealed the mechanisms by which chemotherapy can promote antitumor immunity by induction of immunogenic cell death and disruption of tumor microenvironment components that are used to evade the immune response (Galluzzi et al., 2017; Lutsiak et al., 2005; Michels et al., 2012; Samanta et al., 2018; Tesniere et al., 2010). However, cancer chemotherapies are also considered immunosuppressive owing to their cytotoxic effects on immune cells. Therefore, we speculated that the same chemotherapy may have different impacts on anti-tumor immunity, either stimulatory or inhibitory, depending on the specific combination schedules. We used 5-FU, a common chemotherapeutic agent, as a representative agent to study the influences of different chemotherapeutic and immunotherapeutic combination strategies on the anti-tumor immune response.

Through extensive study of 5-FU-induced immune responses, we revealed both systemic immunosuppressive effects and immune-stimulating effects in the tumor microenvironment. 5-FU treatment upregulated CD80 expression and depleted MDSCs. CD80 is a protein found on antigen-presenting cells as well as tumor cells and belongs to the B7 family; it provides a costimulatory signal necessary for activating T cells and natural killer cells (Beyranvand Nejad et al., 2016; Chambers et al., 1996; Lanier et al., 1995; Singh et al., 2003). Thus, the upregulation of CD80 in tumor tissue induced by 5-FU treatment will potentially lead to increased tumor visibility by T cells. MDSCs are a heterogeneous population of cells that potently suppress T cell responses (Kumar et al., 2016; Veglia et al., 2018). By depleting MDSCs in tumor tissue, 5-FU treatment may potentiate antitumor immunity by eliminating the negative regulations. These findings are also supported by a previous report (Vincent et al., 2010). In addition to the immunogenic effects, we also observed that 5-FU treatment suppressed the T cell population in the tumor microenvironment. Thus, avoiding the immunosuppressive effects and preserving the immunogenic effects of 5-FU treatment will determine the response of 5-FU and immunotherapy combinations.

In our study, the administration of anti-4-1BB or anti-PD-1 after 5-FU treatment significantly improved tumor responses. In this combination strategy, anti-4-1BB or anti-PD-1 selectively boosted response of T cell and NK cells, whereas the 5-FU treatment increased tumor visibility and suppressed MDSCs. However, when anti-4-1BB or anti-PD-1 was added to the repetitive 5-FU treatment, less synergistic effects were observed. Our data highlighted the importance of determining the best schedule for designing a successful chemo-immunotherapy combination. In addition to timing, dosing is another potential factor that affects the chemotherapy-induced immune response. Low-dose chemotherapies have shown special immunoregulatory effects in tumor models (Cao et al., 2014; Ghiringhelli et al., 2007). Further studies are needed to test different chemotherapy doses on the chemo-immunotherapy combination.

In conclusion, our research investigated how traditional cancer treatments will affect novel immunotherapies in clinically relevant tumor models. Our findings indicate that TdLN resection can have adverse impact on anti-tumor immunity, but only in early-stage tumor models. In advanced tumor models, resection of immunotolerant TdLNs during primary tumor surgery does not significantly alter anti-tumor immunity or immunotherapy response in secondary tumors that mimic localized tumor recurrence. Meanwhile, minimizing the immunosuppression and strengthening the immunogenic effects of traditional cancer therapies are critical for immunotherapy-induced durable cancer remission. Specifically, sequential cytotoxic chemotherapy followed by immunotherapy produced a significantly higher degree of anti-tumor response compared with concurrent combination therapy. These findings highlight the need to test immunotherapies in tumor models that more closely mimic different clinical conditions and establish references for designing clinical trials to determine the most effective cancer immunotherapy strategies.

Limitations of the Study

Our pre-clinical studies were mainly performed on mouse tumor models. Although mouse models are heavily used in preclinical studies, mouse tumor development, numbers of tumor-draining lymph nodes, and disease kinetics are different from human clinical conditions. Although we refined our surgical methods and mouse models to closely reflect human conditions, the differences in mouse anatomy and physiology may potentially limit the translational value of our conclusions. Besides, our study was limited only to the commonly used chemotherapies such as 5-FU in pre-clinical models; therefore, further clinical trials are needed to validate our findings acquired in pre-clinical settings.

METHODS

All methods can be found in the accompanying Transparent Methods supplemental file.

SUPPLEMENTAL INFORMATION

Supplemental Information can be found online at https://doi.org/10.1016/j.isci.2020.101056.

ACKNOWLEDGMENTS

This work is supported by the Minnesota Colorectal Cancer Research Funds, Mezin-Koats Colon Cancer Research Award and the ChainBreaker funds from Masonic Cancer Center, University of Minnesota, and University of Minnesota, Medical School Innovation award and the Department of Surgery, Research funds. We thank the Mass Cytometry core facility at University of Minnesota for helpful assistance. We thank Dr. Matthew Robertson and Ms. Isabella Ramirez for assisting with manuscript editing.

AUTHOR CONTRIBUTIONS

X.Z. and S.S. conceived and designed the experiments. X.Z., B.K., and D.W. performed all experiments and data analyses. X.Z., B.K., D.W., E.L., and S.S. commented on the data and co-wrote the paper. S.S. supervised this project.

DECLARATION OF INTERESTS

The authors declare no competing interests.

Received: September 16, 2019
Revised: March 10, 2020
Accepted: April 8, 2020
Published: May 22, 2020

REFERENCES

Beyranvand Nejad, E., van der Sluis, T.C., van Duikeren, S., Yagita, H., Janssen, G.M., van Veelen, P.A., Melief, C.J., van der Burg, S.H., and Arens, R. (2016). Tumor eradication by Cisplatin is sustained by CD80/86-mediated costimulation of CD8+ T cells. Cancer Res. *76*, 6017–6029.

Buchan, S.L., Dou, L., Remer, M., Booth, S.G., Dunn, S.N., Lai, C., Semmrich, M., Teige, I., Martensson, L., Penfold, C.A., et al. (2018). Antibodies to costimulatory receptor 4-1BB enhance anti-tumor immunity via T regulatory cell depletion and promotion of CD8 T cell effector function. Immunity *49*, 958–970.e7.

Cao, Z., Zhang, Z., Huang, Z., Wang, R., Yang, A., Liao, L., and Du, J. (2014). Antitumor and immunomodulatory effects of low-dose 5-FU on hepatoma 22 tumor-bearing mice. Oncol. Lett. *7*, 1260–1264.

Chambers, B.J., Salcedo, M., and Ljunggren, H.G. (1996). Triggering of natural killer cells by the costimulatory molecule CD80 (B7-1). Immunity *5*, 311–317.

Chester, C., Ambulkar, S., and Kohrt, H.E. (2016). 4-1BB agonism: adding the accelerator to cancer immunotherapy. Cancer Immunol. Immunother. *65*, 1243–1248.

Cochran, A.J., Morton, D.L., Stern, S., Lana, A.M., Essner, R., and Wen, D.R. (2001). Sentinel lymph nodes show profound downregulation of antigen-presenting cells of the paracortex: implications for tumor biology and treatment. Mod. Pathol. *14*, 604–608.

Cochran, A.J., Huang, R.R., Lee, J., Itakura, E., Leong, S.P., and Essner, R. (2006). Tumour-induced immune modulation of sentinel lymph nodes. Nat. Rev. Immunol. *6*, 659–670.

DeVita, V.T., Jr., and Chu, E. (2008). A history of cancer chemotherapy. Cancer Res. *68*, 8643–8653.

Emens, L.A., and Middleton, G. (2015). The interplay of immunotherapy and chemotherapy: harnessing potential synergies. Cancer Immunol. Res. *3*, 436–443.

Fend, L., Yamazaki, T., Remy, C., Fahrner, C., Gantzer, M., Nourtier, V., Preville, X., Quemeneur, E., Kepp, O., Adam, J., et al. (2017). Immune checkpoint blockade, immunogenic chemotherapy or IFN-alpha blockade boost the local and abscopal effects of oncolytic virotherapy. Cancer Res. *77*, 4146–4157.

Fisher, B., and Fisher, E.R. (1971). Studies concerning the regional lymph node in cancer. I. Initiation of immunity. Cancer *27*, 1001–1004.

Fransen, M.F., Schoonderwoerd, M., Knopf, P., Camps, M.G., Hawinkels, L.J., Kneilling, M., van Hall, T., and Ossendorp, F. (2018). Tumor-draining lymph nodes are pivotal in PD-1/PD-L1 checkpoint therapy. JCI Insight *3*, 124507.

Galluzzi, L., Buque, A., Kepp, O., Zitvogel, L., and Kroemer, G. (2017). Immunogenic cell death in cancer and infectious disease. Nat. Rev. Immunol. *17*, 97–111.

Ghiringhelli, F., Menard, C., Puig, P.E., Ladoire, S., Roux, S., Martin, F., Solary, E., Le Cesne, A., Zitvogel, L., and Chauffert, B. (2007). Metronomic cyclophosphamide regimen selectively depletes CD4+CD25+ regulatory T cells and restores T and NK effector functions in end stage cancer patients. Cancer Immunol. Immunother. *56*, 641–648.

Gide, T.N., Wilmott, J.S., Scolyer, R.A., and Long, G.V. (2018). Primary and acquired resistance to immune checkpoint inhibitors in metastatic melanoma. Clin. Cancer Res. *24*, 1260–1270.

Ito, M., Minamiya, Y., Kawai, H., Saito, S., Saito, H., Nakagawa, T., Imai, K., Hirokawa, M., and Ogawa, J. (2006). Tumor-derived TGFbeta-1 induces dendritic cell apoptosis in the sentinel lymph node. J. Immunol. *176*, 5637–5643.

Jeanbart, L., Ballester, M., de Titta, A., Corthesy, P., Romero, P., Hubbell, J.A., and Swartz, M.A. (2014). Enhancing efficacy of anticancer vaccines by targeted delivery to tumor-draining lymph nodes. Cancer Immunol. Res. *2*, 436–447.

Kamphorst, A.O., Wieland, A., Nasti, T., Yang, S., Zhang, R., Barber, D.L., Konieczny, B.T., Daugherty, C.Z., Koenig, L., Yu, K., et al. (2017). Rescue of exhausted CD8 T cells by PD-1-targeted therapies is CD28-dependent. Science *355*, 1423–1427.

Kareva, I. (2017). A combination of immune checkpoint inhibition with metronomic chemotherapy as a way of targeting therapy-resistant cancer cells. Int. J. Mol. Sci. *18*, E2134.

Karlsson, M., Marits, P., Dahl, K., Dagoo, T., Enerback, S., Thorn, M., and Winqvist, O. (2010). Pilot study of sentinel-node-based adoptive immunotherapy in advanced colorectal cancer. Ann. Surg. Oncol. *17*, 1747–1757.

Khosravianfar, N., Hadjati, J., Namdar, A., Boghozian, R., Hafezi, M., Ashourpour, M., Kheshtchin, N., Banitalebi, M., Mirzaei, R., and Razavi, S.A. (2018). Myeloid-derived suppressor cells elimination by 5-fluorouracil increased dendritic cell-based vaccine function and

improved immunity in tumor mice. Iran. J. Allergy Asthma Immunol. *17*, 47–55.

Kumar, V., Patel, S., Tcyganov, E., and Gabrilovich, D.I. (2016). The nature of myeloid-derived suppressor cells in the tumor microenvironment. Trends Immunol. *37*, 208–220.

Lake, R.A., O'Hehir, R.E., Verhoef, A., and Lamb, J.R. (1993). CD28 mRNA rapidly decays when activated T cells are functionally anergized with specific peptide. Int. Immunol. *5*, 461–466.

Lanier, L.L., O'Fallon, S., Somoza, C., Phillips, J.H., Linsley, P.S., Okumura, K., Ito, D., and Azuma, M. (1995). CD80 (B7) and CD86 (B70) provide similar costimulatory signals for T cell proliferation, cytokine production, and generation of CTL. J. Immunol. *154*, 97–105.

Le, D.T., Durham, J.N., Smith, K.N., Wang, H., Bartlett, B.R., Aulakh, L.K., Lu, S., Kemberling, H., Wilt, C., Luber, B.S., et al. (2017). Mismatch repair deficiency predicts response of solid tumors to PD-1 blockade. Science *357*, 409–413.

Lee, C.K., Man, J., Lord, S., Links, M., Gebski, V., Mok, T., and Yang, J.C. (2017). Checkpoint inhibitors in metastatic EGFR-mutated non-small cell lung cancer-a meta-analysis. J. Thorac. Oncol. *12*, 403–407.

Linterman, M.A., Denton, A.E., Divekar, D.P., Zvetkova, I., Kane, L., Ferreira, C., Veldhoen, M., Clare, S., Dougan, G., Espeli, M., et al. (2014). CD28 expression is required after T cell priming for helper T cell responses and protective immunity to infection. Elife *3*, e03180.

Liu, J., Blake, S.J., Yong, M.C., Harjunpaa, H., Ngiow, S.F., Takeda, K., Young, A., O'Donnell, J.S., Allen, S., Smyth, M.J., et al. (2016). Improved efficacy of neoadjuvant compared to adjuvant immunotherapy to eradicate metastatic disease. Cancer Discov. *6*, 1382–1399.

Lutsiak, M.E., Semnani, R.T., De Pascalis, R., Kashmiri, S.V., Schlom, J., and Sabzevari, H. (2005). Inhibition of CD4(+)25+ T regulatory cell function implicated in enhanced immune response by low-dose cyclophosphamide. Blood *105*, 2862–2868.

Marzo, A.L., Lake, R.A., Lo, D., Sherman, L., McWilliam, A., Nelson, D., Robinson, B.W., and Scott, B. (1999). Tumor antigens are constitutively presented in the draining lymph nodes. J. Immunol. *162*, 5838–5845.

Michels, T., Shurin, G.V., Naiditch, H., Sevko, A., Umansky, V., and Shurin, M.R. (2012). Paclitaxel promotes differentiation of myeloid-derived suppressor cells into dendritic cells in vitro in a TLR4-independent manner. J. Immunotoxicology *9*, 292–300.

Munn, D.H., and Mellor, A.L. (2006). The tumor-draining lymph node as an immune-privileged site. Immunol. Rev. *213*, 146–158.

Murthy, V., Katzman, D.P., Tsay, J.J., Bessich, J.L., Michaud, G.C., Rafeq, S., Minehart, J., Mangalick, K., de Lafaille, M.A.C., Goparaju, C., et al. (2019). Tumor-draining lymph nodes demonstrate a suppressive immunophenotype in patients with non-small cell lung cancer assessed by endobronchial ultrasound-guided transbronchial needle aspiration: a pilot study. Lung Cancer *137*, 94–99.

Pfirschke, C., Engblom, C., Rickelt, S., Cortez-Retamozo, V., Garris, C., Pucci, F., Yamazaki, T., Poirier-Colame, V., Newton, A., Redouane, Y., et al. (2016). Immunogenic chemotherapy sensitizes tumors to checkpoint blockade therapy. Immunity *44*, 343–354.

Rizvi, N.A., Mazieres, J., Planchard, D., Stinchcombe, T.E., Dy, G.K., Antonia, S.J., Horn, L., Lena, H., Minenza, E., Mennecier, B., et al. (2015). Activity and safety of nivolumab, an anti-PD-1 immune checkpoint inhibitor, for patients with advanced, refractory squamous non-small-cell lung cancer (CheckMate 063): a phase 2, single-arm trial. Lancet Oncol. *16*, 257–265.

Robert, C., Thomas, L., Bondarenko, I., O'Day, S., Weber, J., Garbe, C., Lebbe, C., Baurain, J.F., Testori, A., Grob, J.J., et al. (2011). Ipilimumab plus dacarbazine for previously untreated metastatic melanoma. N. Engl. J. Med. *364*, 2517–2526.

Samanta, D., Park, Y., Ni, X., Li, H., Zahnow, C.A., Gabrielson, E., Pan, F., and Semenza, G.L. (2018). Chemotherapy induces enrichment of CD47(+)/CD73(+)/PDL1(+) immune evasive triple-negative breast cancer cells. Proc. Natl. Acad. Sci. U S A *115*, E1239–E1248.

Sharma, P., Hu-Lieskovan, S., Wargo, J.A., and Ribas, A. (2017). Primary, adaptive, and acquired resistance to cancer immunotherapy. Cell *168*, 707–723.

Shu, S., Cochran, A.J., Huang, R.R., Morton, D.L., and Maecker, H.T. (2006). Immune responses in the draining lymph nodes against cancer: implications for immunotherapy. Cancer Metastasis Rev. *25*, 233–242.

Shuang, Z.-Y., Mao, Y.-Z., Liu, Y.-C., Lin, G.-H., Wang, J.-C., Wang, J., and Li, S.-P. (2017). The tumor-draining lymph nodes are immunosuppressed in patients with hepatocellular carcinoma. Transl. Cancer Res. *6*, 1188–1196.

Singh, N.P., Yolcu, E.S., Taylor, D.D., Gercel-Taylor, C., Metzinger, D.S., Dreisbach, S.K., and Shirwan, H. (2003). A novel approach to cancer immunotherapy: tumor cells decorated with CD80 generate effective antitumor immunity. Cancer Res. *63*, 4067–4073.

Tesniere, A., Schlemmer, F., Boige, V., Kepp, O., Martins, I., Ghiringhelli, F., Aymeric, L., Michaud, M., Apetoh, L., Barault, L., et al. (2010). Immunogenic death of colon cancer cells treated with oxaliplatin. Oncogene *29*, 482–491.

Toki, M.I., Kumar, D., Ahmed, F.S., Rimm, D.L., and Xu, M.L. (2020). Benign lymph node microenvironment is associated with response to immunotherapy. Precision Clin. Med. *3*, 44–53.

Topalian, S.L., Hodi, F.S., Brahmer, J.R., Gettinger, S.N., Smith, D.C., McDermott, D.F., Powderly, J.D., Carvajal, R.D., Sosman, J.A., Atkins, M.B., et al. (2012). Safety, activity, and immune correlates of anti-PD-1 antibody in cancer. N. Engl. J. Med. *366*, 2443–2454.

Vallejo, A.N., Brandes, J.C., Weyand, C.M., and Goronzy, J.J. (1999). Modulation of CD28 expression: distinct regulatory pathways during activation and replicative senescence. J. Immunol. *162*, 6572–6579.

Veglia, F., Perego, M., and Gabrilovich, D. (2018). Myeloid-derived suppressor cells coming of age. Nat. Immunol. *19*, 108–119.

Vincent, J., Mignot, G., Chalmin, F., Ladoire, S., Bruchard, M., Chevriaux, A., Martin, F., Apetoh, L., Rebe, C., and Ghiringhelli, F. (2010). 5-Fluorouracil selectively kills tumor-associated myeloid-derived suppressor cells resulting in enhanced T cell-dependent antitumor immunity. Cancer Res. *70*, 3052–3061.

Wang, N., Wang, Z., Xu, Z., Chen, X., and Zhu, G. (2018). A Cisplatin-loaded immunochemotherapeutic nanohybrid bearing immune checkpoint inhibitors for enhanced cervical cancer therapy. Angew. Chem. *57*, 3426–3430.

Watanabe, S., Deguchi, K., Zheng, R., Tamai, H., Wang, L.X., Cohen, P.A., and Shu, S. (2008). Tumor-induced CD11b+Gr-1+ myeloid cells suppress T cell sensitization in tumor-draining lymph nodes. J. Immunol. *181*, 3291–3300.

Wu, X., Zhang, H., Xing, Q., Cui, J., Li, J., Li, Y., Tan, Y., and Wang, S. (2014). PD-1(+) CD8(+) T cells are exhausted in tumours and functional in draining lymph nodes of colorectal cancer patients. Br. J. Cancer *111*, 1391–1399.

Zhang, L., Dermawan, K., Jin, M., Liu, R., Zheng, H., Xu, L., Zhang, Y., Cai, Y., Chu, Y., and Xiong, S. (2008). Differential impairment of regulatory T cells rather than effector T cells by paclitaxel-based chemotherapy. Clin. Immunol. *129*, 219–229.

Zhao, X., and Subramanian, S. (2017). Intrinsic resistance of solid tumors to immune checkpoint blockade therapy. Cancer Res. *77*, 817–822.

iScience, Volume *23*

Supplemental Information

Chemotherapy but Not the Tumor Draining Lymph Nodes Determine the Immunotherapy Response in Secondary Tumors

Xianda Zhao, Beminet Kassaye, Dechen Wangmo, Emil Lou, and Subbaya Subramanian

Supplemental Figures and Legends

Figure S1

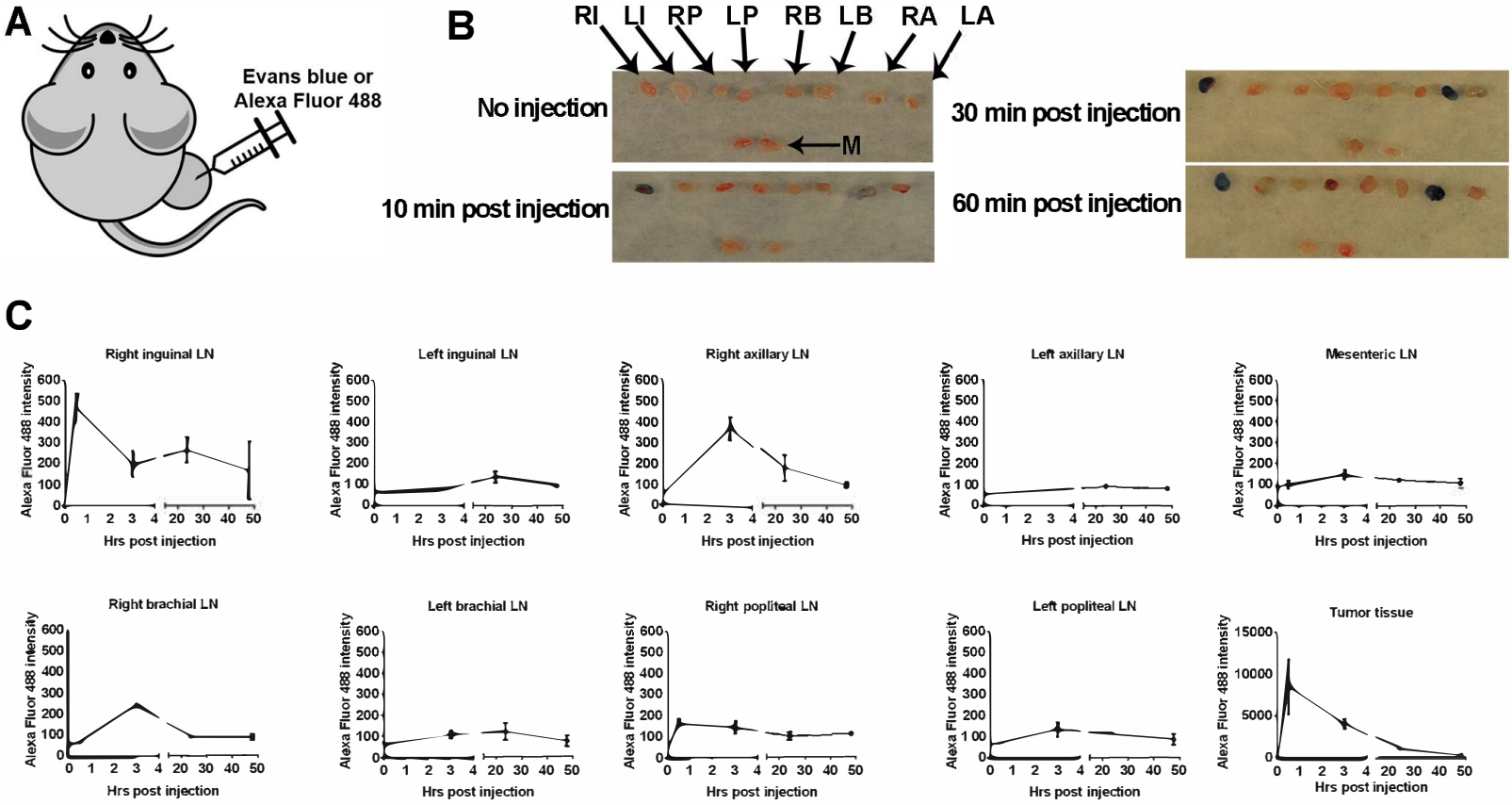

Figure S1. Identification of tumor-draining lymph nodes (TdLNs) in mouse. Related to Figure 1-3.
A) Evan blue dye or Alexa Fluor® 488 dye was injected into the tumor in the right hinge flank to trace TdLNs.
B) 10 min post Evan blue dye injection in the right hinge flank tumor, the right inguinal (RI) and right axillary (RA) lymph nodes (LNs) were stained. The deeper color was seen at 30 min and 60 min post-injection. The representative data from three independent experiments were shown.
C) Flow cytometry was used for detecting the Alexa Fluor® 488 dye distribution in lymphatic organs (drainage from the right hinge flank tumor injection site). The RI LN and RA LN showed the highest FITC signal and were identified as the major TdLNs. The other LNs were identified as the non-draining lymph nodes (NdLNs) (n=3 in each group, data displayed as means ± SEMs, RI: right inguinal, LI: left inguinal, RP: right popliteal, LP: left popliteal, RB: right brachial, LB: left brachial, RA: right axillary, LA: left axillary, M: mesenteric).

Figure S2

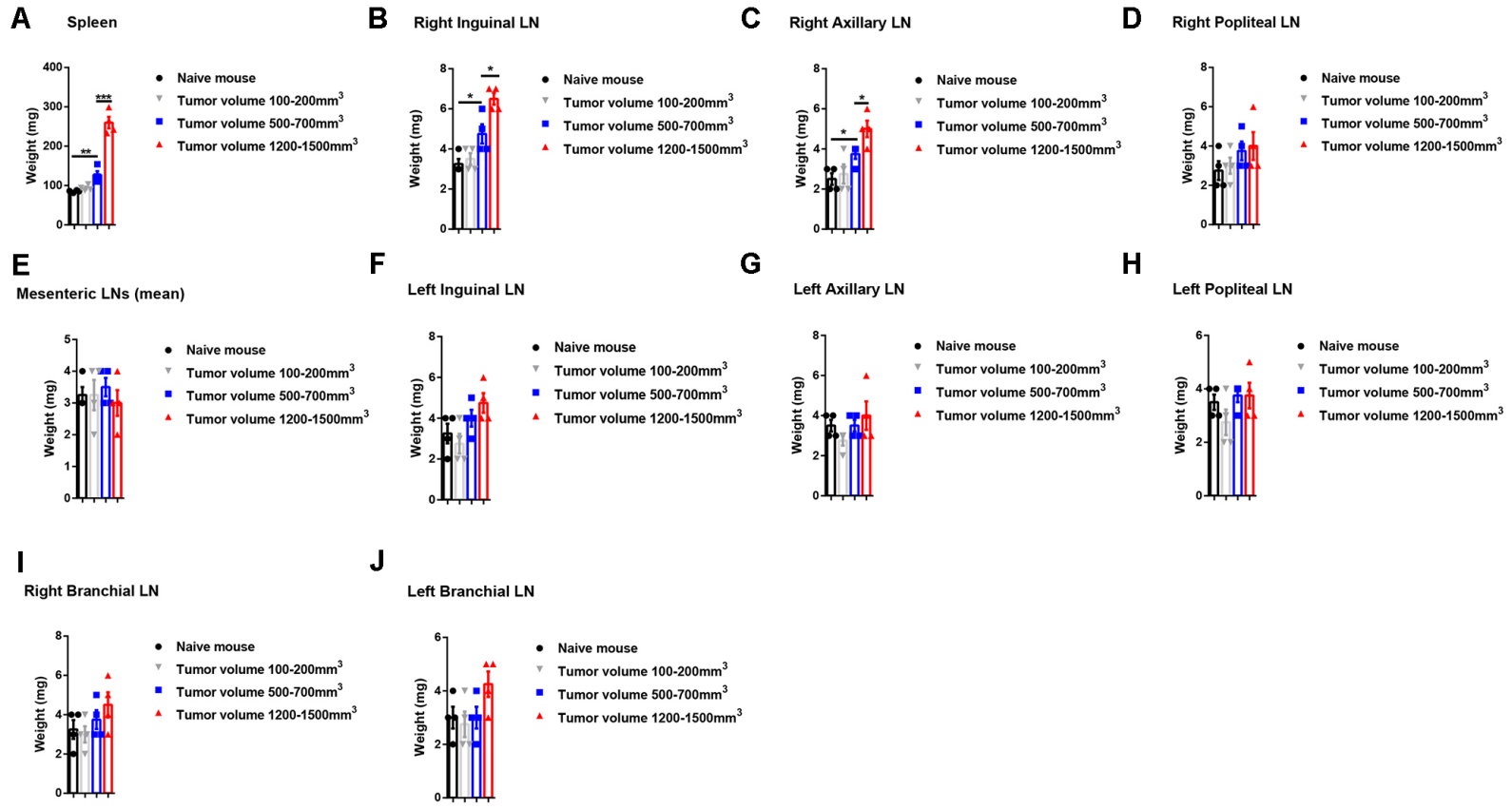
A
Spleen
B
Right Inguinal LN
C
Right Axillary LN
D
Right Popliteal LN
E
Mesenteric LNs (mean)
F
Left Inguinal LN
G
Left Axillary LN
H
Left Popliteal LN
I
Right Branchial LN
J
Left Branchial LN
Weight (mg)
Naive mouse
Tumor volume 100-200mm3
Tumor volume 500-700mm3
Tumor volume 1200-1500mm3

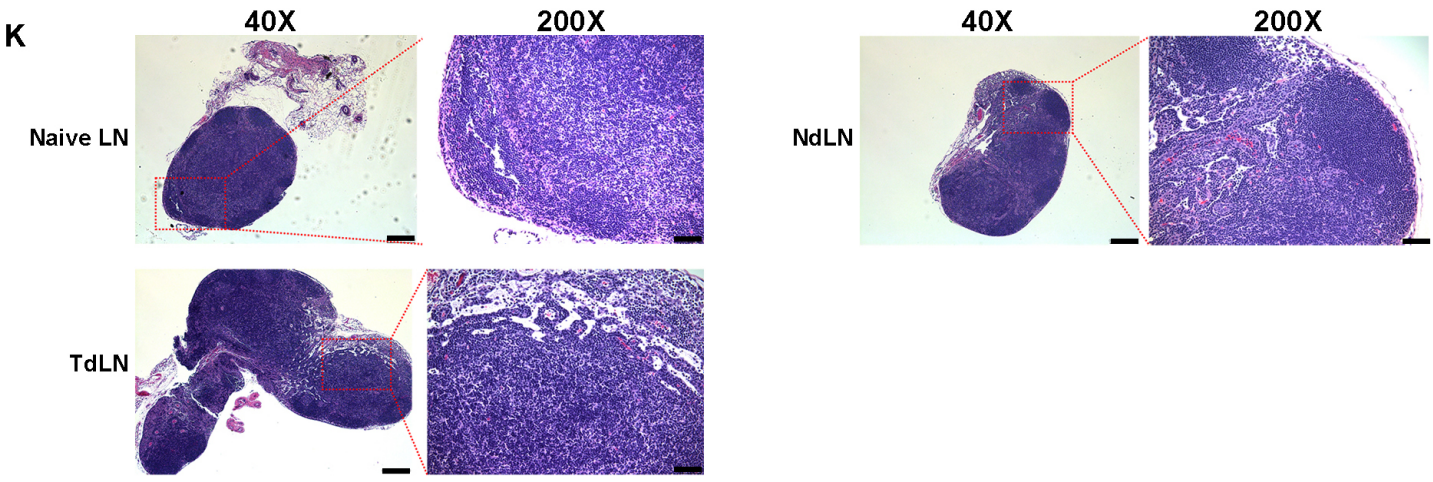
K
40X
200X
Naive LN
TdLN
NdLN

Figure S2. Physical changes and histology of TdLNs, NdLNs, and spleen of tumor-bearing mice. Related to Figure 1-3.

A-J) The weight of spleen and major superficial LNs (both TdLNs and NdLNs) were measured at different time points of tumor development. During tumor development, a significant splenomegaly was observed. An obvious lymphadenopathy was observed in the TdLNs rather than in the NdLNs during tumor development (n=4 in each group, t-test was performed between indicated groups, data were displayed as means ± SEMs, *p<0.05, **p<0.01, ***p<0.001, statistical analyses without significance were not shown).

K) At the late-stage of tumor development, the histology of TdLNs and NdLNs was evaluated. The TdLNs were larger than NdLNs and naïve LNs (taken from tumor-free mice). No metastasis was observed in TdLNs. Representative data from three independent experiments were shown (Scale bars: 250μm in 40X images and 50μm in 200X images).

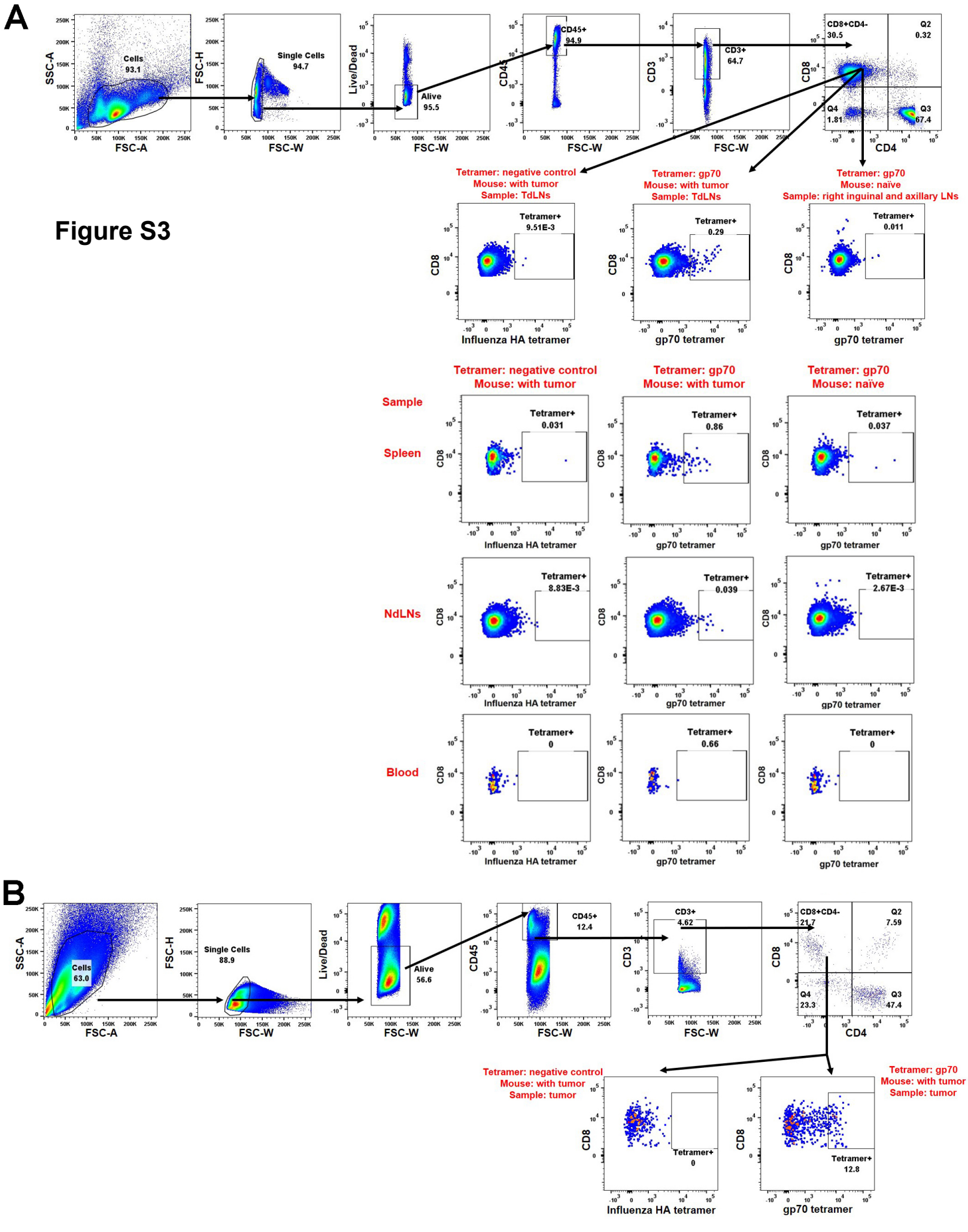
A
SSC-A
FSC-A
Cells
93.1
FSC-H
FSC-W
Single Cells
94.7
Live/Dead
Alive
95.5
CD45
CD45+
94.9
CD3
CD3+
64.7
CD8
CD4
CD8+CD4-
30.5
Q2
0.32
Q4
1.81
Q3
67.4
Tetramer: negative control
Mouse: with tumor
Sample: TdLNs
Tetramer: gp70
Mouse: with tumor
Sample: TdLNs
Tetramer: gp70
Mouse: naïve
Sample: right inguinal and axillary LNs
Tetramer+
9.51E-3
0.29
0.011
Influenza HA tetramer
gp70 tetramer
Figure S3
Sample
Spleen
NdLNs
Blood
0.031
0.86
0.037
8.83E-3
0.039
2.67E-3
0
0.66
B
Cells
63.0
Single Cells
88.9
Alive
56.6
CD45+
12.4
CD3+
4.62
CD8+CD4-
21.7
Q2
7.59
Q4
23.3
Q3
47.4
Tetramer: negative control
Mouse: with tumor
Sample: tumor
Tetramer: gp70
Mouse: with tumor
Sample: tumor
12.8

Figure S3. Gating of tumor antigen-specific $CD8^+$ T cells. Related to Figure 1 and 3.
A) Representative gating process of $CD8^+$ gp70 (tumor) antigen-specific T cells in peripheral lymphatic organs.
B) Representative gating process of $CD8^+$ gp70 (tumor) antigen-specific T cells in tumor tissues. The negative tetramer and lymphatic organs from naïve mice were used as controls for gating.

Figure S4

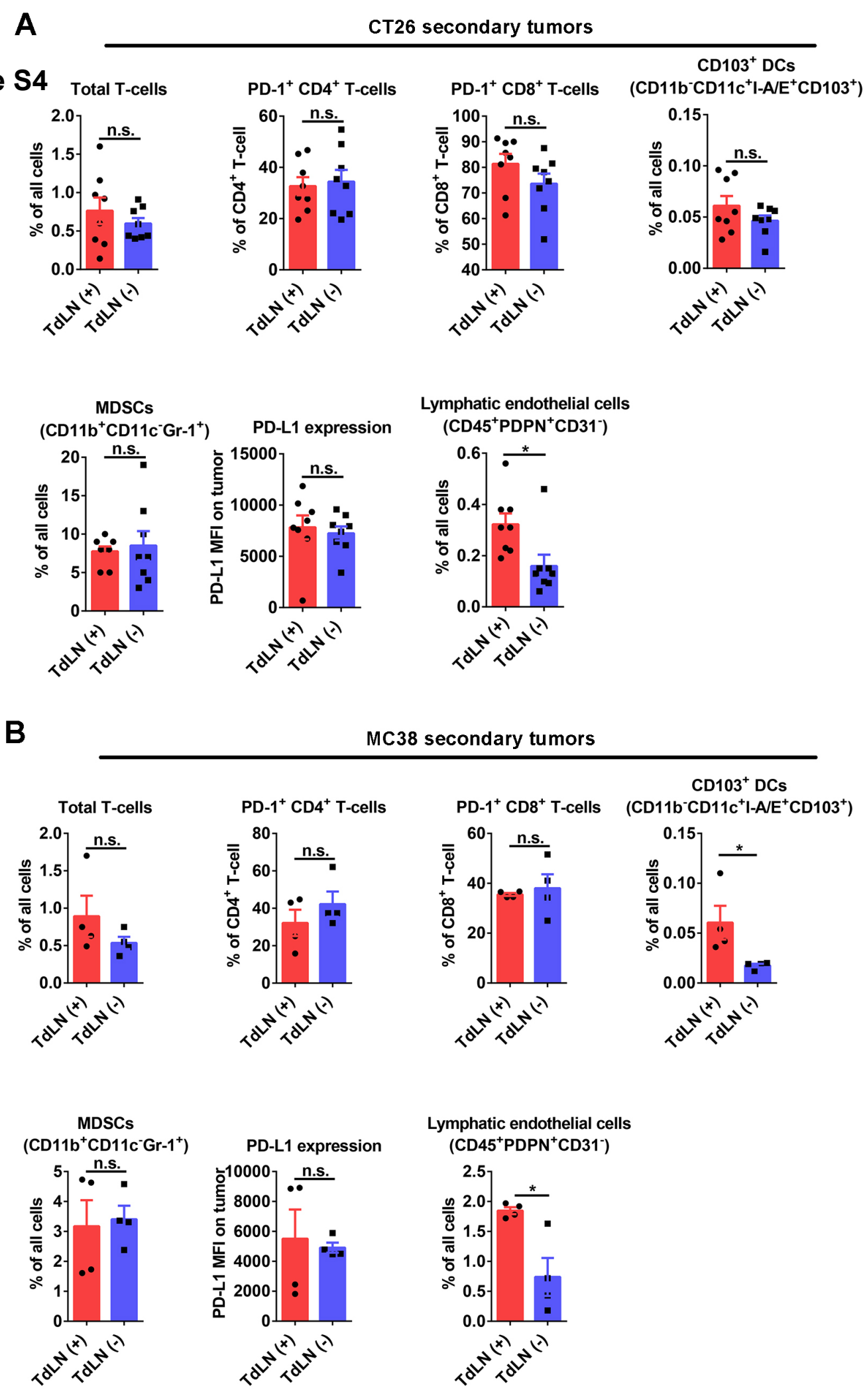
A
CT26 secondary tumors
Total T-cells
% of all cells
n.s.
PD-1+ CD4+ T-cells
% of CD4+ T-cell
n.s.
PD-1+ CD8+ T-cells
% of CD8+ T-cell
n.s.
CD103+ DCs
(CD11b-CD11c+I-A/E+CD103+)
% of all cells
n.s.
MDSCs
(CD11b+CD11c-Gr-1+)
% of all cells
n.s.
PD-L1 expression
PD-L1 MFI on tumor
n.s.
Lymphatic endothelial cells
(CD45+PDPN+CD31-)
% of all cells
*
TdLN (+)
TdLN (-)
B
MC38 secondary tumors
Total T-cells
% of all cells
n.s.
PD-1+ CD4+ T-cells
% of CD4+ T-cell
n.s.
PD-1+ CD8+ T-cells
% of CD8+ T-cell
n.s.
CD103+ DCs
(CD11b-CD11c+I-A/E+CD103+)
% of all cells
*
MDSCs
(CD11b+CD11c-Gr-1+)
% of all cells
n.s.
PD-L1 expression
PD-L1 MFI on tumor
n.s.
Lymphatic endothelial cells
(CD45+PDPN+CD31-)
% of all cells
*
TdLN (+)
TdLN (-)

Figure S4. Immune features in secondary tumors with or without TdLNs. Related to Figure 2.
A) The frequency of lymphatic endothelia cells was higher in CT26 secondary tumors (mimicking recurrent tumors) with TdLNs than secondary tumors without TdLNs (n=8 in each group, t-test). The total tumor-infiltrating T cell frequency, PD-1 high expression T cells frequency, $CD103^+$ dendritic cells (DCs) frequency, myeloid-derived suppressive cells (MDSCs) frequency, and PD-L1 expression were similar in two groups (n=8 in each group, t-test was performed, data displayed as means ± SEMs, n.s.: no significance, *p<0.05).
B) The experiments were repeated in the MC38 tumor model. The frequency of lymphatic endothelial cells and $CD103^+$ DCs were higher in secondary tumors with TdLNs than in secondary tumors without TdLNs (n=4 in each group, t-test was performed, data displayed as means ± SEMs, n.s.: no significance, *p<0.05).

Figure S5

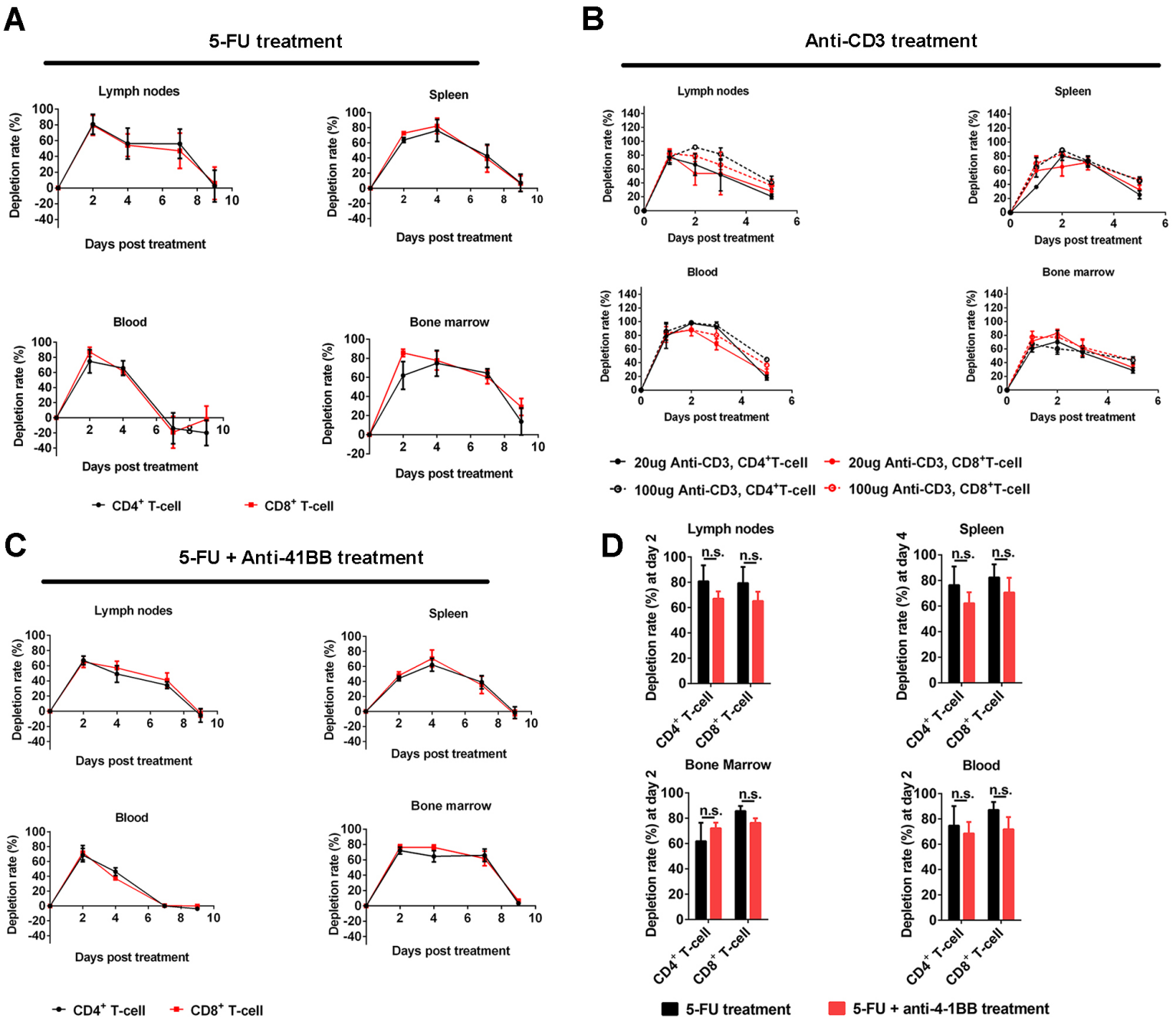
A
5-FU treatment
Lymph nodes
Spleen
Blood
Bone marrow
Depletion rate (%)
Days post treatment
CD4+ T-cell
CD8+ T-cell
B
Anti-CD3 treatment
20ug Anti-CD3, CD4+T-cell
20ug Anti-CD3, CD8+T-cell
100ug Anti-CD3, CD4+T-cell
100ug Anti-CD3, CD8+T-cell
C
5-FU + Anti-41BB treatment
D
Depletion rate (%) at day 2
Depletion rate (%) at day 4
Bone Marrow
n.s.
5-FU treatment
5-FU + anti-4-1BB treatment

Figure S5. T cell depleting effects of 5-FU and anti-CD3 treatment. Related to Figure 2 and 4-6.
A) 5-FU treatment on naïve mice depleted T cells in lymphatic organs, blood circulation, and bone marrow. The T cell population was recovered around 9 days after 5-FU treatment (n=3 in each group, data were displayed as means ± SEMs).
B) Single-dose of anti-CD3 treatment on naïve mice depleted T cells for around 3 days (n=3 in each group, data were displayed as means ± SEMs).
C-D) A combination of anti-4-1BB with 5-FU didn't rescue the T cell depletion induced by 5-FU treatment (n=3 in each group, t-test was performed, data were displayed as means ± SEMs, n.s.: no significance).

Figure S6

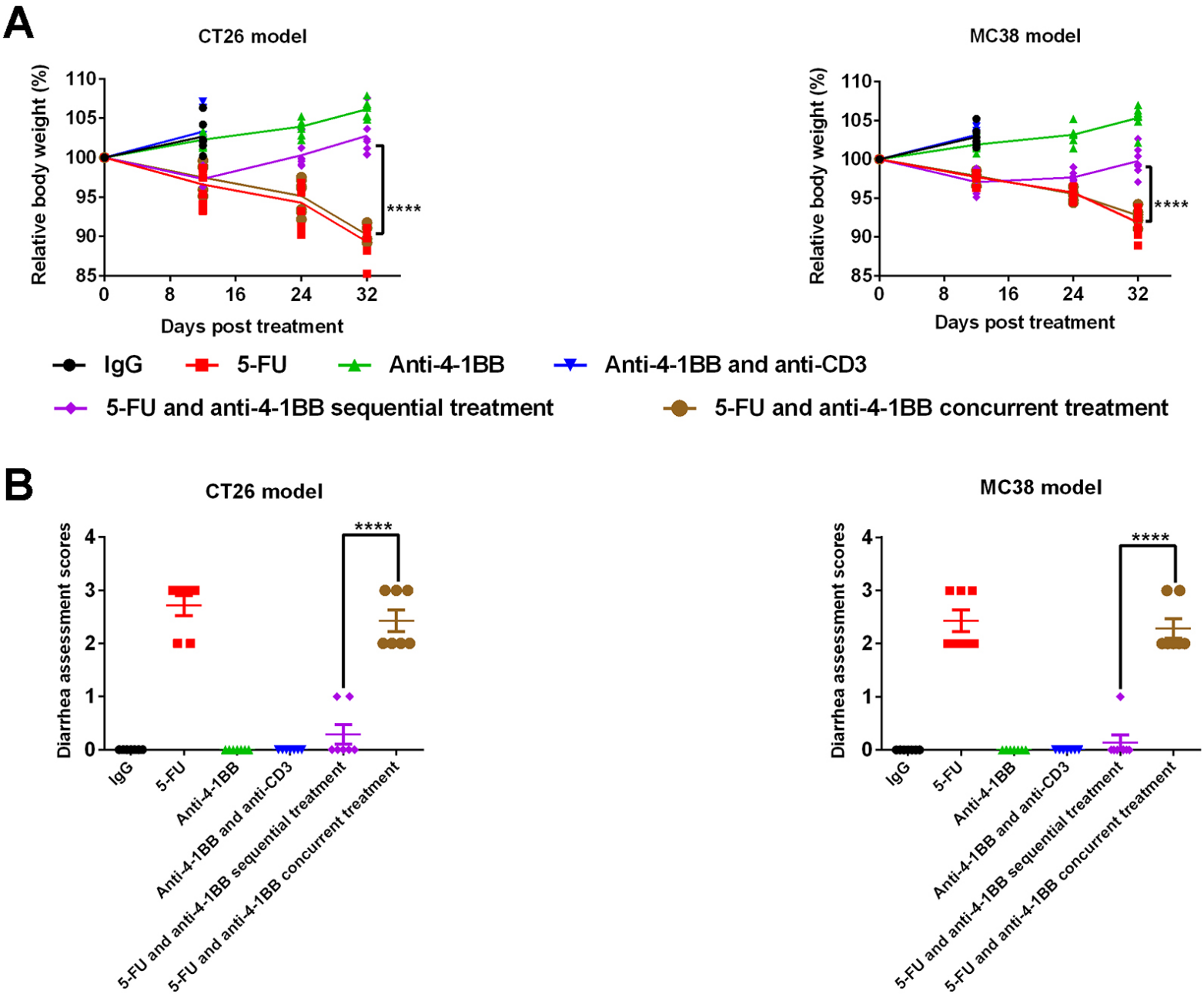
A
CT26 model
MC38 model
Relative body weight (%)
110
105
100
95
90
85
0
8
16
24
32
Days post treatment
****
IgG
5-FU
Anti-4-1BB
Anti-4-1BB and anti-CD3
5-FU and anti-4-1BB sequential treatment
5-FU and anti-4-1BB concurrent treatment
B
CT26 model
MC38 model
Diarrhea assessment scores
4
3
2
1
0
****
IgG
5-FU
Anti-4-1BB
Anti-4-1BB and anti-CD3
5-FU and anti-4-1BB sequential treatment
5-FU and anti-4-1BB concurrent treatment

Figure S6. Side effects of different treatments. Related to Figure 4.

A-B) The mouse body weight was measured on day 12, 24, and 32 during treatment (related to figure 4). On day 32, the mice treated with the 5-FU and anti-4-1BB sequential treatment have higher body weight than the mice treated with the 5-FU and anti-4-1BB concurrent treatment (n=7 in each group, t-test was performed between indicated groups at the last time point, individual value was shown, ****$p<0.0001$).

C-D) Diarrhea assessment was performed at the endpoint of mice follow-up to evaluate the side effects on mouse intestine. The 5-FU and anti-4-1BB concurrent but not sequential treatment caused severe diarrhea (n=7 in each group, t-test was performed between indicated groups, data were displayed as means ± SEMs, ****$p<0.0001$).

Figure S7

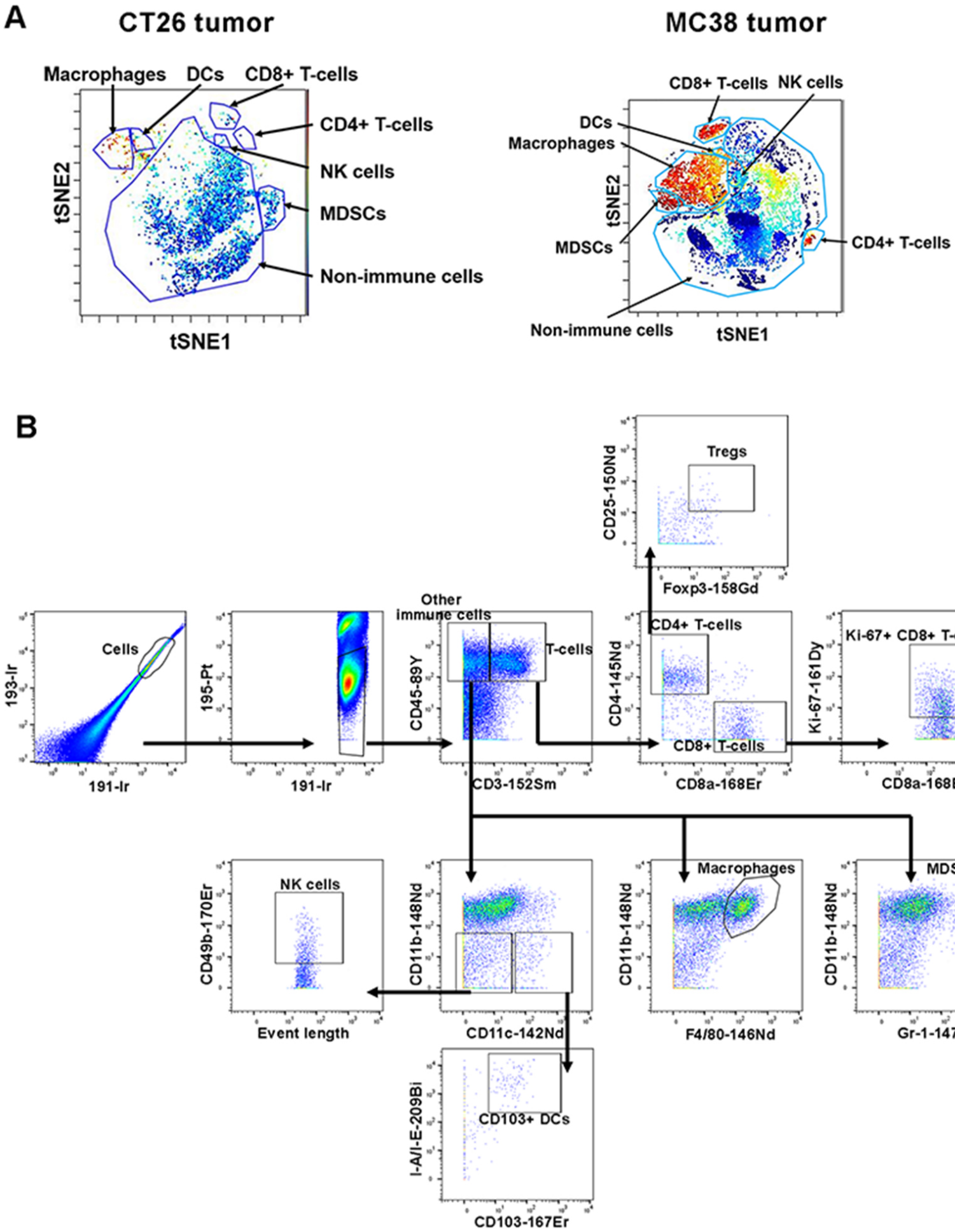
A
CT26 tumor
Macrophages
DCs
CD8+ T-cells
CD4+ T-cells
NK cells
MDSCs
Non-immune cells
tSNE2
tSNE1
MC38 tumor
CD8+ T-cells
NK cells
DCs
Macrophages
MDSCs
CD4+ T-cells
Non-immune cells
tSNE2
tSNE1
B
Cells
193-Ir
191-Ir
195-Pt
191-Ir
Other immune cells
T-cells
CD45-89Y
CD3-152Sm
CD25-150Nd
Tregs
Foxp3-158Gd
CD4+ T-cells
CD4-145Nd
CD8+ T-cells
CD8a-168Er
Ki-67+ CD8+ T-cells
Ki-67-161Dy
CD8a-168Er
NK cells
CD49b-170Er
Event length
CD11b-148Nd
CD11c-142Nd
CD103+ DCs
I-A/I-E-209Bi
CD103-167Er
Macrophages
CD11b-148Nd
F4/80-146Nd
MDSCs
CD11b-148Nd
Gr-1-147Sm

Figure S7. Gating of the tumor-infiltrating immune cells. Related to Figure 6.

A) The major tumor-infiltrating immune cell populations were showed in the ViSNE plots.

B) Manual gating of the major tumor-infiltrating immune cells. The alive cell population was first identified and the immune cells ($CD45^+$) were then gated. The gating of T-cell populations ($CD45^+CD3^+CD8^+$ for $CD8^+$ T cells, $CD45^+CD3^+CD4^+CD25^+Foxp3^+$ for T_{regs}), NK cells ($CD45^+CD3^-CD11b^-CD11c^-CD49b^+$), macrophages ($CD45^+CD3^-CD11b^+F4/80^+$), myeloid-derived suppressive cells (MDSCs, $CD45^+CD3^-CD11b^+Gr\text{-}1^+$), and $CD103^+$ DCs ($CD45^+CD3^-CD11b^-CD11c^+$I-A/I-$E^+CD103^+$) were showed here. The same markers were used throughout the study to identify the immune cells.

Figure S8

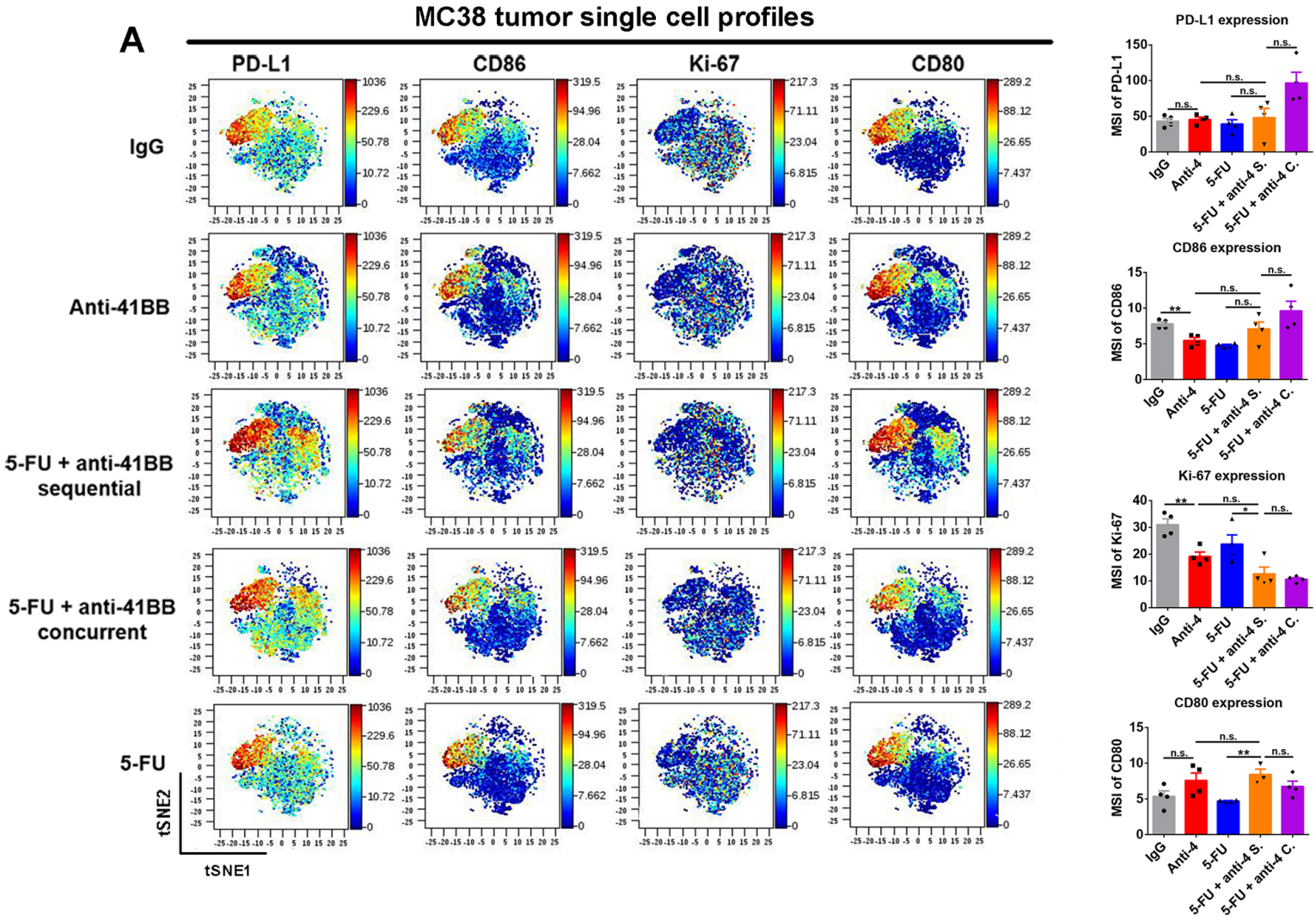
A
MC38 tumor single cell profiles
PD-L1
CD86
Ki-67
CD80
IgG
Anti-41BB
5-FU + anti-41BB sequential
5-FU + anti-41BB concurrent
5-FU
tSNE2
tSNE1
PD-L1 expression
MSI of PD-L1
CD86 expression
MSI of CD86
Ki-67 expression
MSI of Ki-67
CD80 expression
MSI of CD80
IgG
Anti-4
5-FU
5-FU + anti-4 S.
5-FU + anti-4 C.

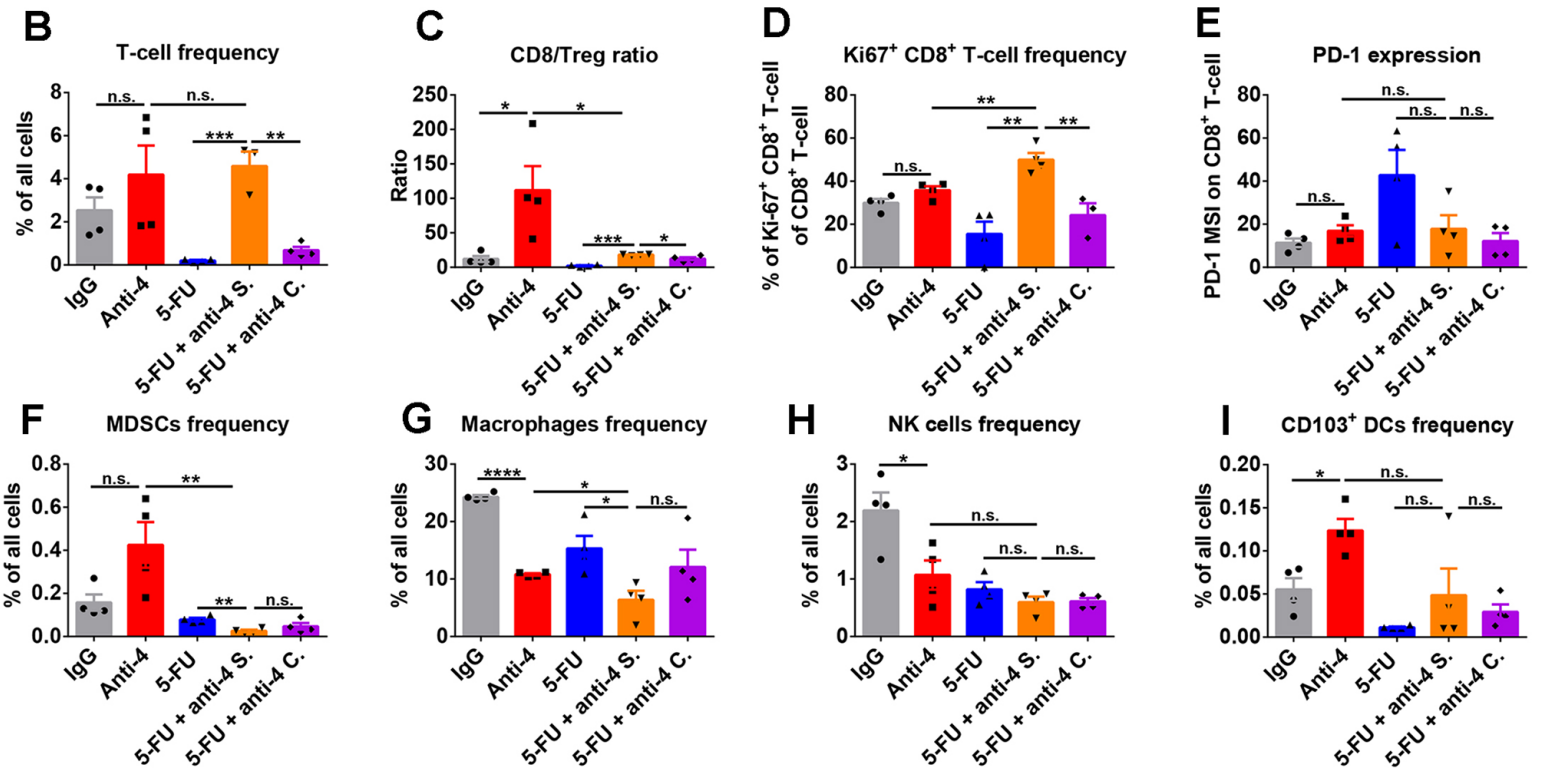
B
T-cell frequency
% of all cells
C
CD8/Treg ratio
Ratio
D
Ki67+ CD8+ T-cell frequency
% of Ki-67+ CD8+ T-cell of CD8+ T-cell
E
PD-1 expression
PD-1 MSI on CD8+ T-cell
F
MDSCs frequency
% of all cells
G
Macrophages frequency
% of all cells
H
NK cells frequency
% of all cells
I
CD103+ DCs frequency
% of all cells
IgG
Anti-4
5-FU
5-FU + anti-4 S.
5-FU + anti-4 C.

Figure S8. Tumor immunological response to 5-FU and anti-4-1BB treatments in MC38 tumors. Related to Figure 6.

A) ViSNE plot showed single cell level expression of PD-L1, Ki-67, CD80, and CD86 in the MC38 tumor tissue. The 5-FU and anti-4-1BB sequential treatment significantly upregulated CD80 while decreased Ki-67 expression in tumor tissues (n=4 in each group, t-test was performed between indicated groups, data were displayed as means ± SEMs, MSI: mean signal intensity, n.s.: no significance, *p<0.05, **p<0.01).

B-I) The tumor-infiltrating T cell frequency, CD8/Treg ratio, and Ki-67^+ $CD8^+$ T cell frequency were higher in the sequential treatment than the concurrent treatment group. The myeloid-derived suppressive cells (MDSCs) were depleted in 5-FU treated groups. The 5-FU and anti-4-1BB sequential treatment were compared with the anti-4-1BB monotherapy, 5-FU monotherapy, and 5-FU and anti-4-1BB concurrent treatment (n=4 in each group, t-test was performed between indicated groups, data were displayed as means ± SEMs, MSI: mean signal intensity, n.s.: no significance, *p<0.05, **p<0.01, *** p<0.001, ****p<0.0001).

Figure S9

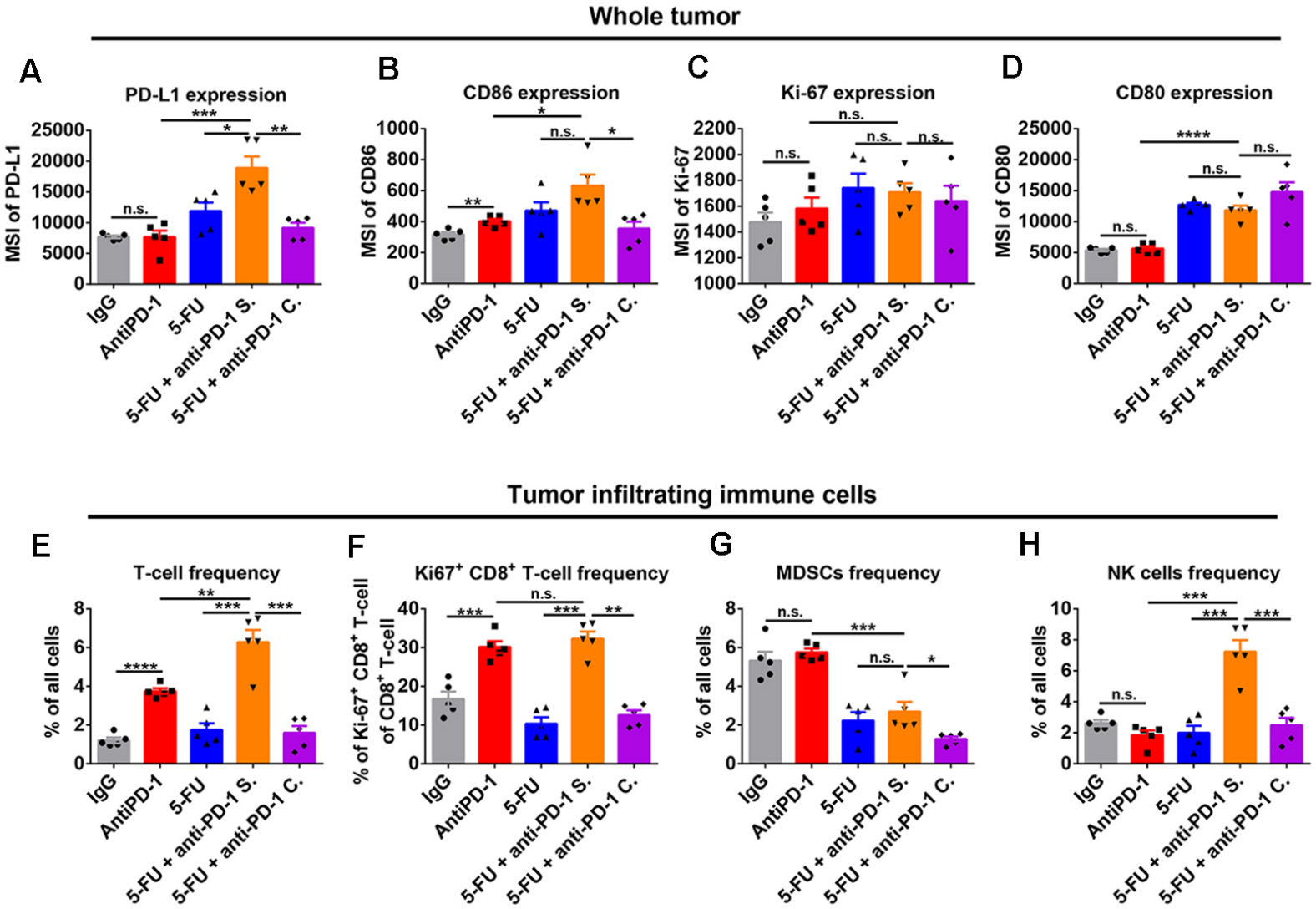
Whole tumor
A
PD-L1 expression
MSI of PD-L1
B
CD86 expression
MSI of CD86
C
Ki-67 expression
MSI of Ki-67
D
CD80 expression
MSI of CD80
IgG
AntiPD-1
5-FU
5-FU + anti-PD-1 S.
5-FU + anti-PD-1 C.
Tumor infiltrating immune cells
E
T-cell frequency
% of all cells
F
Ki67+ CD8+ T-cell frequency
% of Ki-67+ CD8+ T-cell of CD8+ T-cell
G
MDSCs frequency
% of all cells
H
NK cells frequency
% of all cells

Figure S9. Tumor immunological response to 5-FU and anti-PD-1 treatments in CT26 tumors. Related to Figure 6.

A-D) The 5-FU and anti-PD-1 sequential treatment significantly increased PD-L1, CD80, and CD86 expression in CT26 tumors (n=5 in each group, t-test was performed between indicated groups, data were displayed as means ± SEMs, MSI: mean signal intensity, n.s.: no significance, *p<0.05, **p<0.01, *** p<0.001, ****p<0.0001).

E-H) The 5-FU and anti-PD-1 sequential treatment significantly increased tumor-infiltrating T cell frequency, Ki-$67^{+}CD8^{+}$ T cell frequency, and NK cell frequency in tumor tissues, compared with the concurrent treatment. The myeloid-derived suppressive cells (MDSCs) were depleted in 5-FU treated groups (n=5 in each group, t-test was performed between indicated groups, data were displayed as means ± SEMs, MSI: mean signal intensity, n.s.: no significance, *p<0.05, **p<0.01, *** p<0.001, ****p<0.0001).

Table S1. gp70 mRNA expression in different tissues. Related to Figure 1-3.

Model	Tumor tissue	Tumor marginal skin & connective tissues post-surgery	Normal skin tissue
CT26 (Babl/c)	Positive	Negative	Negative
MC38 (C57BL/6)	Positive	Negative	Negative

Transparent Methods

Cell cultures

Murine CRC cell lines CT26 (purchased from American Type Culture Collection (ATCC)) and MC38 (gift from Dr. Nicholas Haining) were used for the study and were authenticated by STR profiling. CT26 cells were maintained in complete RPMI-1640 medium (GIBCO BRL), supplemented with 10% heat-inactivated FBS (Thermo Fisher Scientific), 100 IU/mL penicillin, and 100 µg/mL streptomycin (Invitrogen Life Technologies). MC38 cells were cultured in the complete DMEM medium (GIBCO BRL) with the same supplements as the RPMI 1640 medium. All cells were routinely authenticated and tested for mycoplasma.

Mice

Wild type BALB/c mice (6-8 weeks old, Jackson Laboratory) and C57BL/6 mice (6-8 weeks old, Charles River Laboratories) were used for animal studies. All mice were kept in a specific pathogen-free facility with fully autoclaved cages to minimize non-tumor specific immune activation. Animal studies were approved by the institutional animal care and use committee (IACUC). All mice are female. We don't expect the any influence of gender on our study aims.

Subcutaneous tumor induction

For the subcutaneous syngeneic model, the cells were harvested at low passages, washed, and resuspended in Matrigel matrix (Corning Inc.) before injection. Mice were shaved right before injection. CT26 (2×10^5 cells/injection) or MC38 (5×10^5 cells/injection) cells were inoculated subcutaneously into the right hind-flank of 6 to 8-week-old female BALB/c or C57BL/6 mice. The same amount of tumor cells were used for the rechallenge experiment in Figure 1. Tumor length and width were measured every three to seven days, and the volume was calculated according to the formula (length × width^2)/2. Mice were divided into different experimental groups at random when tumors reached a specific size.

Identification of major tumor-draining lymph nodes

To identify the major tumor-draining lymph nodes (TdLNs), we injected 50µl 1% Evans blue (Sigma-Aldrich) or 50µl 1% Alexa Fluor® 488 dye (Thermo Fisher Scientific) into the subcutaneous tumor (~400-500mm^3) at the right hind flank. The left and right inguinal LNs, axillary LNs, brachial LNs, popliteal LNs, and mesentery LNs were taken at 10 min, 30 min, and 60 min post Evan blue injection. For the fluorescence-labeled group, we collected LNs at 0.5h, 3h, 24h, and 48h post-injection. The intact LNs were visually examined for Evans blue staining. LNs, spleen, and tumor tissues were ground and meshed for single cell suspension, which was measured by flow cytometry for Alexa Fluor® 488 dye signal. To evaluate the physical change of LNs and spleen during tumor development, we weighted LNs and spleen from naïve mice and mice with different sizes of the tumor (100-200mm^3, 500-700mm^3, or 1200-1500mm^3).

Subcutaneous tumor and TdLNs resection

Primary tumors were resected when they reached the indicated volume as shown in the experimental schematics in each figure. Tumor-bearing mice were anesthetized with Ketamine (100 mg/kg) and Xylazine (10 mg/kg) by intraperitoneal injection. To minimize animal pain, we administrated Buprenorphine (slow-releasing, 2 mg/kg) subcutaneously 2 hours before anesthesia. Mice were prepared by removing hair from the skin region over the tumor. We prepared the skin by wiping with iodine prep pads and then alcohol prep pads. Resections were performed by elliptical incisions, 5mm left to the subcutaneous tumors. With iris scissors, we separated the capsule of subcutaneous tumors from the surrounding connective tissue to isolate and resect intact tumors. Once tumors were removed from the adjacent fascia, the incisions were sutured with 5/0 vicryl ties (polyglactin 910, Ethicon). For the TdLNs resection, the TdLNs were located based on the superficial anatomic landmark points. The mice were prepared as mentioned above. A 5-10mm incision was made and TdLNs were removed. Then the skin was sutured with 5/0 vicryl ties. For tumor rechallenge, 1 day after surgery, we inoculated the secondary tumor (CT26: 5×10^5 cells/injection, MC38: 1×10^6 cells/injection) to the surgical site to mimic tumor recurrence.

RT-qPCR

We used the murine leukemia virus envelope gp70 as a biomarker of tumor burden. Biopsies were collected from normal mouse skin, tumor tissue, and surgical margin after tumor resection. The mirVana microRNA (miRNA) Isolation Kit (Thermo Fisher Scientific) was used to extract total RNA from these biopsies. 500 ng of total RNA was used for establishing the cDNA library with the QuantiTect Reverse Transcription Kit (Qiagen). We used the LightCycler 480 Instrument (Roche Life Science) to measure 18S ribosomal RNA (rRNA) and gp70 expression.

Primers used: 18S rRNA forward primer: GTTGGTTTTCGGAACTGAGG, 18S rRNA reverse primer: AGTCGGCATCGTTTATGGTC, gp70 forward primer: AAAGTGACACATGCCCACAA, gp70 reverse primer: CCCCAAGAGGCACAATAGAA(Scrimieri et al., 2013).

Flow cytometry

Flow cytometry was used to measure tumor tissue immune infiltration, tumor antigen-specific T cells, and immune cell functions. Harvested tumor tissues were chopped into small pieces (around 3mm x 3mm) and then digested in a solution of collagenase IV (1 mg/ml) and deoxyribonuclease (DNase, 50 units/ml) at 37°C for 1 hr with shaking. The digested tissue was then meshed and filtered through a 70 μm cell strainer. The cell suspension was centrifuged and resuspended in red blood cell lysis buffer for 15 minutes at room temperature (RT) for eliminating red blood cells. Another centrifugation was performed to get the cell pellet for staining. For the lymphatic organs, we directly meshed the tissue and filtered through a 40 μm cell strainer to get single cell suspension, followed by red blood cells elimination.

Following the tissue sample preparation, cells were stained with the fixable cell viability dye and then cell surface marker antibodies for a 15 min incubation at 4°C. Next, cells were fixed and permeabilized for intracellular staining for a 30 min incubation at RT. The cells were finally stained with intracellular markers (30 min at RT) and analyzed on a BD FACS-CANTO instrument (BD Biosciences). To analyze the tumor antigen-specific T cells, we performed H-2Ld MuLV gp70-SPSYVYHQF APC conjugated tetramer (MBL International) staining by following the manufacturer's instruction, before antibody staining. The influenza hemagglutinin-IYSTVASSL APC conjugated tetramer (MBL International), which should only stain a very minimal population of T cells in mice without influenza hemagglutinin stimulation, was used as a negative control for ruling out false positive in the tetramer staining and setting up the gate for gp70 tetramer. Lymphatic tissues from naïve mice were also used as negative controls. According to the manufacture's instruction and our preliminary experiment optimization, we used anti-CD8 (clone KT15) antibody (MBL International) to further reduce false-positive rate of the tetramer staining. All antibodies for flow cytometry were purchased from Biolegend and summarized in supplementary materials. Data were analyzed using FlowJo software (Tree Star, Inc.).

Mass cytometry

Details on antibodies and reagents used are listed in materials table. We purchased the prelabeled antibodies from Fluidigm Corporation and unlabeled antibodies (MaxPar® Ready purified) from Biolegend. Conjugation of the purified antibodies with metal tags was performed by using the MaxPar X8 antibody labeling kit (Fluidigm Corporation) according to the manufacturer's instructions. The metal tagged antibodies were then validated and titrated in positive control and negative control samples.

Tumor samples were collected and digested using standard flow cytometry procedure. A total of 3 million single cells were used for each mass cytometry staining. In brief, the single cell pellets were first incubated with Cell-ID Cisplatin with a final concentration of 5 μM for 5 min at RT to identify dead cells. Cells were then washed and blocked by Fc-receptor blocking solution. Cell membrane staining was then performed with metal-conjugated antibodies for 30 min at RT. After staining, cells were fixed and permeabilized. The intracellular staining antibodies were then added and incubated for 45 min at RT. Finally, cells were labeled with 1 ml 1,000× diluted 125 μM Cell-ID intercalator-Ir to stain all cells in MaxPar Fix and Perm Buffer overnight at 4 °C. EQ Four Element Calibration Beads with the reference EQ passport P13H2302 were added to each staining tube right before data acquisition by a CyTOF 2 mass cytometer. The mass cytometry data were then normalized and exported for gating on alive single cells, which were then imported to the Cytobank software. A t-SNE analysis was performed with default parameters (perplexity, 30; iterations, 1,000) on all cell types in tumor samples.

Mouse IFN-γ enzyme-linked immunosorbent assays

Mouse naïve lymph nodes and TdLNs were collected, weighed, and ground in 100 μl RIPA lysis and extraction buffer. After the tissues were lysed, the total protein was used for enzyme-linked immunosorbent assay (ELISA, Affymetrix) to detect mouse *IFNγ*, by following the manufacturer's protocol.

Histology

Mouse naïve lymph nodes, TdLNs, and non-tumor draining lymph nodes (NdLNs) were collected and fixed in 10% formalin for 24 hr. Tissues were embedded in paraffin and cut for hematoxylin and eosin (H&E) staining. The whole tissue sections were scanned and analyzed for potential metastatic tumor cells.

T cell depletion

We tested the effects of 5-FU treatment and 5-FU and anti-4-1BB combination treatment on T cell depletion *in vivo*. Intraperitoneal administration of anti-CD3 treatment (clone: 17A2, BioXcell, 5 mg/kg every 3 days) was given to induce T cell depleted mice. One dose of 5-FU (150 mg/kg) or 5-FU (150 mg/kg) and anti-4-1BB (5 mg/kg) combination treatment was given intraperitoneally in naïve mice. Mice were sampled on days 2, 4, 7, and 9 after treatment for quantifying T cells in lymph nodes, spleen, bone marrow, and blood circulation.

Mouse treatments

Mice were treated with IgG (5 mg/kg as an anti-4-1BB control, 10 mg/kg as an anti-PD-1 control), 5-FU (150 mg/kg), anti-4-1BB agonist (5 mg/kg, clone: 3H3), or anti-PD-1 (10 mg/kg, clone: RMP1-14) for treatment purpose. For the 5-FU monotherapy, one dose of 5-FU was given every 12 days to minimize the severe side effects. For anti-4-1BB and IgG monotherapy, mice were treated every 3 days. For the 5-FU and anti-4-1BB sequential treatment, anti-4-1BB treatment started 9 days after one dose 5-FU treatment and continued as 3 days per injection after that. For the 5-FU and anti-4-1BB concurrent treatment, we added the anti-4-1BB cycle to the 5-FU cycle. The anti-PD-1 was used as the same as the anti-4-1BB cycle. All treatments were given intraperitoneally and continued until the endpoint of study design. The treatment starting points and endpoints varied in different experiments for different purposes and were shown in the individual figure or figure legend.

5-FU toxicity evaluation

We recorded animal body weight and diarrhea scores after treatments. Mice were weighed on day 12, 24, and 32 after treatment. The diarrhea score was assessed at the endpoint of each treatment by using a 4-point scoring system: 0=normal stool; 1=slight diarrhea (soft formed stool without perianal staining of the coat); 2=moderate diarrhea (unformed stool with moderate perianal staining of the coat); and 3=severe diarrhea (watery stool with severe perianal staining of the coat)(Song et al., 2013).

Statistical analysis

All statistical analyses and graphing were performed using GraphPad Prism software (Version 6). Data were displayed as means ± SEMs. For comparison of two groups quantitative data, paired or unpaired Student's t-test was performed. When applicable, one-way analysis of variance (ANOVA) was utilized for multiple groups' comparison, followed by post hoc (Tukey's) multiple comparisons test. Kaplan-Meier curves were plotted to visualize mouse survival, and log-rank tests were used to compare survival outcomes between subgroups. A two-tail P value of less than 0.05 was considered statistically significant.

Table of key materials

Reagent for immune assays	**Clone**	**Vendor**	**Identifier**
Anti-mouse CD3-FITC	17A2	BioLegend	100204
Anti-mouse CD28-PE	37.51	BioLegend	102106
Anti-mouse PD-1-PerCP/Cy5.5	29F.1A12	BioLegend	135208
Anti-mouse CD62L-PE/Cy7	MEL-14	BioLegend	104418
Anti-mouse CD8a-APC/Cy7	53-6.7	BioLegend	100714
Anti-mouse LAG-3-BV421	C9B7W	BioLegend	125221
Anti-mouse/human CD44-PE	IM7	BioLegend	103008
Anti-mouse CD19-Pacific Blue	6D5	BioLegend	115523
Anti-mouse CD4-BV510	GK1.5	BioLegend	100449
Anti-mouse CD86-PE	GL-1	BioLegend	105007
Anti-mouse F4/80-PE/Cy5	BM8	BioLegend	123111
Anti-mouse CD80-PE/Cy7	16-10A1	BioLegend	104734
Anti-mouse/human CD11b-APC	M1/70	BioLegend	101212
Anti-mouse I-A/I-E-APC/Cy7	M5/114.15.2	BioLegend	107628
Anti-mouse CD11c-BV510	N418	BioLegend	117338
Anti-mouse CD45-Pacific Blue	30-F11	BioLegend	103126
Anti-mouse CD45-FITC	30-F11	BioLegend	103108
Anti-mouse CD3-PerCP/Cyanine5.5	17A2	BioLegend	100218
Anti-mouse CD3ε-PE/Cy7	145-2C11	BioLegend	100320

Anti-mouse CD103-Pacific Blue	2E7	BioLegend	121418
Anti-mouse Gr-1-PE/Cy7	RB6-8C5	BioLegend	108416
Anti-mouse CD45-BV510	30-F11	BioLegend	103138
Anti-mouse Podoplanin-APC/Cy7	8.1.1	BioLegend	127418
Anti-mouse CD31-Pacific Blue	390	BioLegend	102422
Anti-mouse CD45-89Y	30-F11	Fluidigm	3089005B
Anti-mouse Ly-6G-41Pr	1A8	Fluidigm	3141008B
Anti-mouse CD11c-142Nd	N418	Fluidigm	3142003B
Anti-mouse CD4-145Nd	RM4-5	Fluidigm	3145002B
Anti-mouse F4/80-146Nd	BM8	Fluidigm	3146008B
Anti-mouse Gr-1-147Sm	RB6-8C5	BioLegend/Fluidigm	108449/201147B
Anti-mouse CD11b-148Nd	M1/70	Fluidigm	3148003B
Anti-mouse CD19-149Sm	6D5	Fluidigm	3149002B
Anti-mouse CD25-150Nd	3C7	Fluidigm	3150002B
Anti-mouse CD28-151Eu	37.51	Fluidigm	3151005B
Anti-mouse CD3e-152Sm	145-2C11	Fluidigm	3152004B
Anti-mouse CD274-153Eu	10F.9G2	Fluidigm	3153016B
Anti-mouse CD152-154Sm	UC10-4B9	Fluidigm	3154008B
Anti-mouse CD279-155Gd	RMP1-30	BioLegend/Fluidigm	109113/201155A
Anti-mouse CD335-156Gd	29A1.4	BioLegend/Fluidigm	137625/201156B
Anti-mouse Foxp3-158Gd	FJK-16s	Fluidigm	3158003A
Anti-mouse RORgt-B2D-159Tb	B2D	Fluidigm	3159019B
Anti-mouse CD62L-160Gd	MEL-14	Fluidigm	3160008B
Anti-mouse Ki-67-161Dy	B56	Fluidigm	3161007B
Anti-mouse Ly-6C-162Dy	HK1.4	Fluidigm	3162014B
Anti-mouse CD197-164Dy	4B12	Fluidigm	3164013A
Anti-mouse IFNg-165Ho	XMG1.2	Fluidigm	3165003B
Anti-mouse IL-4-166Er	11B11	Fluidigm	3166003B
Anti-mouse CD103-167Er	2E7	BioLegend/Fluidigm	121402/ 201167B
Anti-mouse CD8a-168Er	53-6.7	Fluidigm	3168003B
Anti-mouse CD49b-170Er	HMa2	Fluidigm	3170008B
Anti-mouse CD80-171Yb	16-10A1	Fluidigm	3171008B
Anti-mouse CD86-172Yb	GL1	Fluidigm	3172016B
Anti-mouse Granzyme B-173Yb	GB11	Fluidigm	3173006B
Anti-mouse CD127-174Yb	A7R34	Fluidigm	3174013B
Anti-mouse CD44-176Yb	IM7	BioLegend/Fluidigm	103051/201176B
Anti-mouse I-A/I-E-209Bi	M5/114.15.2	Fluidigm	3209006B
Cell-ID™ Intercalator-Ir	NA	Fluidigm	201192B
Cell-ID™ Cisplatin	NA	Fluidigm	201064
H-2Ld MuLV gp70 Tetramer-APC	NA	MBL International	TB-M521-2
IFN gamma Mouse ELISA Kit	NA	Thermo Fisher Scientific	BMS606
Zombie Violet™ Fixable Viability Kit	NA	BioLegend	423113
Zombie Aqua™ Fixable Viability Kit	NA	BioLegend	423101
Zombie Green™ Fixable Viability Kit	NA	BioLegend	423111
MuLV gp70 Tetramer-APC	NA	MBL International	TB-M521-2
Influenza HA Tetramer-APC	NA	MBL International	TS-M520-2
Anti-mouse CD8-FITC	KT15	MBL International	D271-4
Drugs or antibodies for treatment	**Clone**	**Vendor**	**Identifier**
Anti-mouse 4-1BB (CD137)	3H3	BioXcell	BE0239
Anti-mouse PD-1	RMP1-14	BioXcell	BP0146
Anti-mouse CD3	17A2	BioXcell	BE0002
5-Fluorouracil	NA	Intas Pharmaceuticals	DB00544

Mouse	**Age**	**Vendor**	**Identifier**
BALB/cJ	6-8 weeks	The Jackson Laboratory	000651
C57BL/6	6-8 weeks	Charles River	027

Supplemental References

Scrimieri, F., Askew, D., Corn, D.J., Eid, S., Bobanga, I.D., Bjelac, J.A., Tsao, M.L., Allen, F., Othman, Y.S., Wang, S.C.*, et al.* (2013). Murine leukemia virus envelope gp70 is a shared biomarker for the high-sensitivity quantification of murine tumor burden. Oncoimmunology *2*, e26889.

Song, M.K., Park, M.Y., and Sung, M.K. (2013). 5-Fluorouracil-induced changes of intestinal integrity biomarkers in BALB/c mice. Journal of cancer prevention *18*, 322-329.